UCRL-19244

cy. 2

NONLEPTONIC DECAY OF SIGMA HYPERONS

Roger Odell Bangerter
(Ph.D. Thesis)

July 7, 1969

AEC Contract No. W-7405-eng-48

UCRL-19244
cy. 2

LAWRENCE RADIATION LABORATORY
UNIVERSITY of CALIFORNIA BERKELEY

DISCLAIMER

NONLEPTONIC DECAY OF SIGMA HYPERONS

Contents

Abstract v

I. Introduction 1

II. Beam Design 6

A. Design Requirements 6

B. Septum Separator 8

C. Beam Optics 11

III. Determination of P_Σ 16

IV. Measurement of the α Parameters 20

A. Scanning and Measuring Biases 20

B. Contamination of Sample 31

C. Measurement of α 35

V. Measurement of the Φ Parameters 43

A. Identification of Events 45

B. Estimation of Background 48

C. Investigation of Biases 52

D. Maximum Likelihood Determination of Φ 55

VI. Theoretical Analysis and Conclusions 60

Acknowledgments 75

Appendices 76

A. Resolution of the $\Sigma_o^+ - \Sigma_+^+$ Ambiguity 76

B. Monte Carlo Simulation of np Scattering Background 81

C. A Theorem on the Distribution of $\chi_m^2 - \chi_n^2$ 84

Contents (Continued)

D. Preliminary Measurements of Decay Rates 88

References 94

NONLEPTONIC DECAY OF SIGMA HYPERONS

Roger Odell Bangerter

Lawrence Radiation Laboratory
University of California
Berkeley, California

July 7, 1969

ABSTRACT

In this dissertation we present measurements of the decay parameters α_-, α_o and α_+ for $\Sigma^- \to n\pi^-$, $\Sigma^+ \to p\pi^o$, and $\Sigma^+ \to n\pi^+$. We have also measured the decay parameters Φ_- and Φ_+ for $\Sigma^- \to n\pi^-$ and $\Sigma^+ \to n\pi^+$. The usual decay parameters α, β, and γ are related to Φ by the equations $\beta = (1 - \alpha^2)^{\frac{1}{2}} \sin \Phi$ and $\gamma = (1 - \alpha^2)^{\frac{1}{2}} \cos \Phi$.

Polarized $\Sigma^\pm$ are produced by the reaction $K^- p \to \Sigma^\pm \pi^\mp$ in the Lawrence Radiation Laboratory's 25-inch hydrogen bubble chamber. The average momentum of the incident K^- beam is 385 MeV/c. The measurements of α are performed by observing the up-down asymmetry in the Σ decay distributions and the measurements of Φ are made by observing the left-right asymmetry in the np interactions of those decay neutrons that subsequently scattered on the hydrogen in the bubble chamber.

We obtain $\alpha_- = -0.071 \pm 0.012$, $\alpha_o = -0.999 \pm 0.022$, $\alpha_+/\alpha_o = -0.062 \pm 0.016$, $\Phi_- = 14 \pm 19$ deg, and $\Phi_+ = 143 \pm 29$ deg. These results are in agreement with the $|\Delta I| = 1/2$ rule.

I. INTRODUCTION

"Happy is the man that findeth wisdom, and the man that getteth understanding.
For the merchandise of it is better than the merchandise of silver, and the gain thereof than fine gold."
Proverbs 3:13-14

Since their discovery in the early 1950's the nonleptonic Σ decays $\Sigma^{\pm} \to n\pi^{\pm}$ and $\Sigma^{+} \to p\pi^{o}$ have been vigorously studied both experimentally and theoretically. Unfortunately, we are not yet in a position where wisdom and understanding can be said to characterize the state of our knowledge. In an effort to ameliorate this situation we present new experimental data constituting a significant statistical improvement over previous results. Our data are relevant to a number of theoretical suggestions.

As early as 1954 Gell-Mann and Pais[1] noted that the decays of all the recently-discovered hyperons seemed to obey a $|\Delta I| = 1/2$ rule. This rule has subsequently been shown to be satisfied at least approximately by all strangeness changing weak processes. However, the dynamical reasons for the existence of this rule in nonleptonic processes are obscure. One of the major purposes of this dissertation is to examine the $|\Delta I| = 1/2$ rule in light of our new data.

We will also briefly discuss the relationship of our data to time reversal invariance and the current algebra results of Sugawara and Suzuki.[2]

By way of further introduction we give a brief exposition of nonleptonic Σ decay phenomenology, a survey of the current experimental situation, and a discussion of the history and motivation of our experi-

ment.

Both the initial state Σ and final state nucleon have $J^P = 1/2^+$ while the pion has $J^P = 0^-$. Thus only s and p orbital states are allowed, and nonleptonic Σ decay can be completely parameterized in terms of two complex numbers s and p representing the amplitudes for the two orbital states. In terms of the Pauli spin formalism the decay matrix element is written as

$$T = U_N^\dagger \, (s + p \, \vec{\sigma}\cdot\hat{q}) \, U_\Sigma$$

where $\hat{q}$ is a unit vector along the direction of the decay nucleon in the Σ rest frame.

For convenience, rather than s and p, nonleptonic hyperon decays are conventionally parameterized in terms of their decay rates Γ and the three parameters α, β, and γ defined as

$$\alpha = \frac{2\mathrm{Re}\,(s^* p)}{|s|^2 + |p|^2} \tag{1}$$

$$\beta = \frac{2\mathrm{Im}\,(s^* p)}{|s|^2 + |p|^2} \tag{2}$$

$$\gamma = \frac{|s|^2 - |p|^2}{|s|^2 + |p|^2} \tag{3}$$

Since $\alpha^2 + \beta^2 + \gamma^2 = 1$ it is further convenient to introduce an additional parameter Φ defined by

$$\beta = (1 - \alpha^2)^{1/2} \sin \Phi$$

$$\gamma = (1 - \alpha^2)^{1/2} \cos \Phi \, .$$

Also the likelihood function for Φ is more nearly Gaussian than that for β or γ. A subscript +, -, or 0 will be used on all parameters to indicate the charge of the decay pion.

Table I is a summary of the previous experimental information.[3] Published data that are a subset of the data presented in this dissertation have been excluded from this summary. The branching ratio is denoted by b.

Table I

Reaction	α	Φ	Γ_{total}	b
$\Sigma^- \rightarrow n\pi^-$	$-.106 \pm .039$	$-22^o \pm 30^o$	$(.604 \pm .011) \times 10^{10}$/sec	1.00
$\Sigma^+ \rightarrow p\pi^o$	$-.829 \pm .135$		$(1.235 \pm .020) \times 10^{10}$/sec	$0.528 \pm .015$
$\Sigma^+ \rightarrow n\pi^+$	$\alpha_+/\alpha_o = -.022 \pm .059$	$180^o \pm 30^o$	$(1.235 \pm .020) \times 10^{10}$/sec	$0.472 \pm .015$

The decay distribution in the Σ rest frame is given by the familiar expression

$$I(\cos\theta)\, d(\cos\theta) = 1/2\,(1 + \alpha P_\Sigma \cos\theta)\, d(\cos\theta). \qquad (4)$$

where P_Σ is the polarization of the Σ and $\cos\theta = \vec{P}_\Sigma \cdot \hat{q}$.

The polarization of the nucleon is given by

$$\vec{P}_N = \left\{ \left[\alpha + (1-\gamma)\vec{P}_\Sigma \cdot \hat{q} \right] \hat{q} + \gamma \vec{P}_\Sigma + \beta(\vec{P}_\Sigma \times \hat{q}) \right\} / (1 + \alpha \vec{P}_\Sigma \cdot \hat{q}) \,. \qquad (5)$$

In 1963 Watson, Ferro-Luzzi, and Tripp[4] published the results of their hydrogen bubble chamber experiment on the K^-p interaction between 250 and 513 MeV/c. They showed that in the vicinity of 390 MeV/c the reactions $K^-p \rightarrow \Sigma^\pm \pi^\mp$ are a copious source ($\sim$ 20 mb) of highly polarized

Σ hyperons. Furthermore P_Σ can be accurately calculated on the basis of a reliable partial-wave analysis. It was soon recognized that it would be possible to do a hydrogen bubble chamber experiment to measure α_o, $\alpha_\pm$, and $\Phi_\pm$. In each case α can be determined by measuring distribution (4). Apart from measured kinematical quantities, $\vec{P}_n$ is dependent on α, $\vec{P}_\Sigma$, and Φ. Since both α and $\vec{P}_\Sigma$ can be determined independently of (5), $\vec{P}_n$ becomes a function of the single unknown parameter Φ. The polarization $\vec{P}_n$, and hence Φ, is measured by observing the left-right asymmetry in the np interactions of those decay neutrons that subsequently scatter on the hydrogen in the bubble chamber. Figure 1 illustrates the complete sequence of reactions for a Σ^- event.

No accurate measurement of Φ_o is possible in such an experiment since the pp interaction provides very poor analysis of $\vec{P}_n$.

Our experiment was proposed in May 1964. During the period from August 1965 to September 1967, we obtained about 1.3×10^6 pictures using the Lawrence Radiation Laboratory's 25-inch hydrogen bubble chamber. There are approximately 6 K^- per frame yielding 60 000 Σ^- events and 80 000 Σ^+ events. The average K^- momentum is about 385 MeV/c.

In Section II we discuss the design and construction of our experiment. Section III treats the partial-wave analysis and the determination of P_Σ. Sections IV and V explain the measurement of α and Φ. Finally in Section VI we discuss the theoretical implications of our experiment, particularly its relevance to the $|\Delta I| = 1/2$ rule.

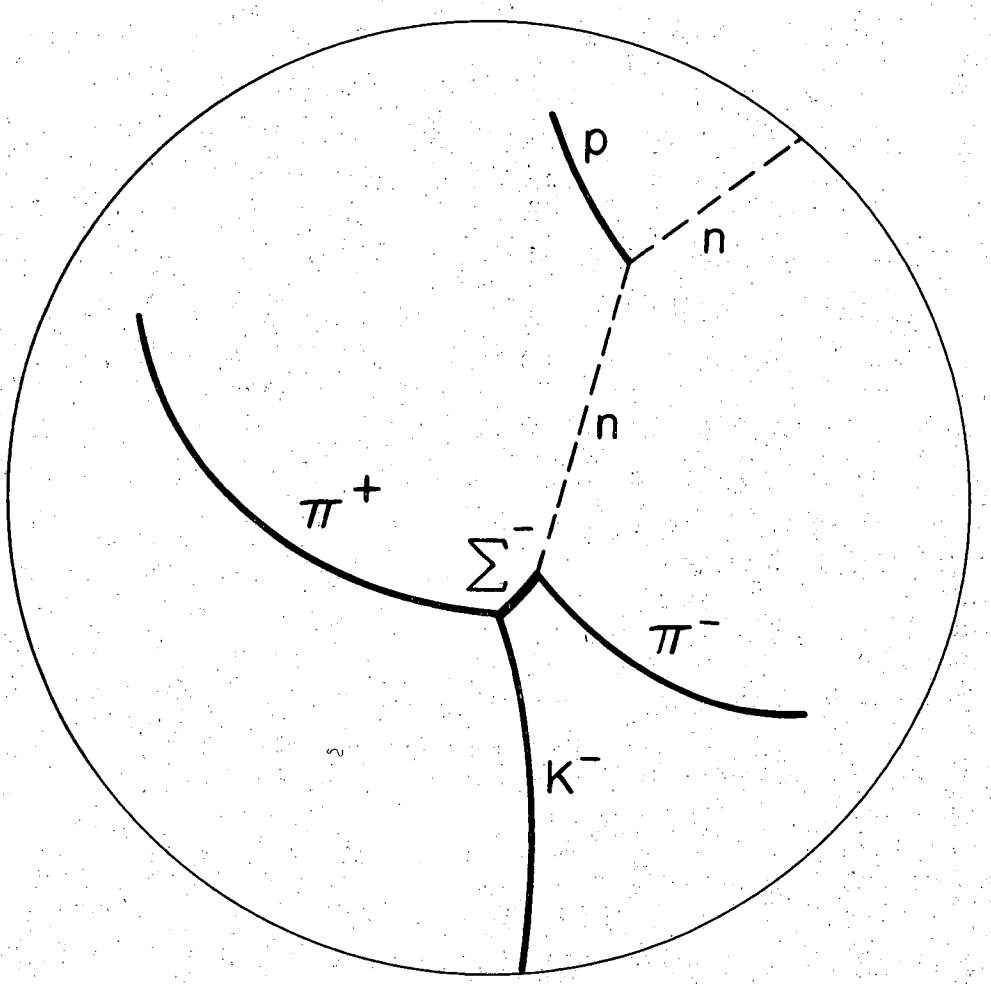

XBL696-3136

Fig. 1. Typical Σ^- event with np scattering.

II. BEAM DESIGN

A. Design Requirements

In June of 1964 we began the difficult task of actually building a 400 MeV/c K^- beam. It seems that there is a conspiracy in nature to prevent one from building such a beam at the Bevatron. In the first place K^- production at this momentum is very low. This is true both absolutely and also in comparison to other particles. The production rate for background particles (mostly electrons and pions) is about three orders of magnitude larger than K^- production. In addition K^- decay losses amount to about 10% per foot. The background, however, decays relatively slowly causing the ratio of K^- to background to deteriorate rapidly as the beam is made longer. On the other hand a high background normally requires multi-stage electrostatic separation, which in turn requires a long beam. And finally, although the pions decay slowly, they do decay rapidly enough to badly contaminate the beam with muons.

As a specific example of these difficulties, the Alvarez group had previously performed a 450 MeV/c K^- experiment at the Bevatron. The beam was located in the 76° area of Quad III and was 39 feet in length. It had an angular acceptance of about .5 millisteradian, a momentum acceptance of ± 2%, and a transmission efficiency for K^- of roughly 25%. This beam yielded approximately .25 K^- per 10^{10} protons. A single stage coaxial separator[5] was used giving a background to K^- ratio of 65:1.

As a further example, a study has been made which shows that a

compact optical system could be used with two short conventional separators to achieve a 40-foot beam. Unfortunately the background would still be an order of magnitude larger than the K^- intensity.

Since the 76^o Quad III location of the Bevatron was already equipped with the vacuum channel suitable for the extraction of low momentum particles, we chose this area as the site for our beam. We adopted the criterion of 10 K^- tracks per frame as our design goal. For reasons of compatability with other experiments, and in order to minimize radioactivation of the Bevatron, it is undesirable to use more than about 10^{12} protons per pulse. The maximum angular and momentum acceptance of the beam is largely determined by the size of the vacuum channel. Assuming then the same acceptance and transmission efficiency as the previous Alvarez group experiment, one sees by comparison that the beam cannot be made much longer than about 40 feet and still yield an adequate K^- flux. With conventional techniques our beam is impossible.

Taking into account both production and decay rates and assuming a beam length of 40 feet the ratio of background to K^- at the bubble chamber would be 50 000:1. What is needed then is a short separator capable of rejections of better than 10^5:1. It should be designed in such a way that it removes the background as early in the beam as possible to prevent μ contamination from π decay. Accordingly Joseph J. Murray proposed a scheme for such a separator, a so-called septum separator, which, in its present form is more of a filter than a separator.

B. Septum Separator

The operation of the separator can be understood by reference to Figure 2. The solid lines represent the paths of K^- particles and the dashed lines the paths of π^- and e^- particles. The deflection of a particle in an electric field goes as 1/(momentum x velocity). Thus the pions and electrons are deflected less than the K^- particles and strike the uranium bars U_1 at p or the stainless steel electrodes at q. This entire sequence occurs again in the last two sets of electrodes so we effectively have two-stage separation. Our calculations and experiments indicate that particles represented by the dotted lines can scatter off of the electrodes with little energy loss. In this way large numbers of pions and electrons could propagate through the system. They are obstructed by the uranium bars U_1. Those pions and electrons which just graze the edge at point p (or miss it entirely) will be found preferentially in the position occupied by the uranium bars U_2. These bars materially lower the background without affecting K^- transmission. Note that the vertical scale in Figure 2 has been greatly magnified. Figure 3 is a photograph of one of the four sets of electrodes actually used in the experiment.

Since the effective gap for K^- transmission is only about .050 inches and the length of the separator is about 80 inches, the beam must be parallel to better than .050/80 = .625 milliradian and must also be aimed parallel to the axis of the separator with this order of precision. These requirements demanded some special attention as is discussed in the next section. It should be noted that the .050-inch effective gap results in a maximum transmission efficiency of 25% since

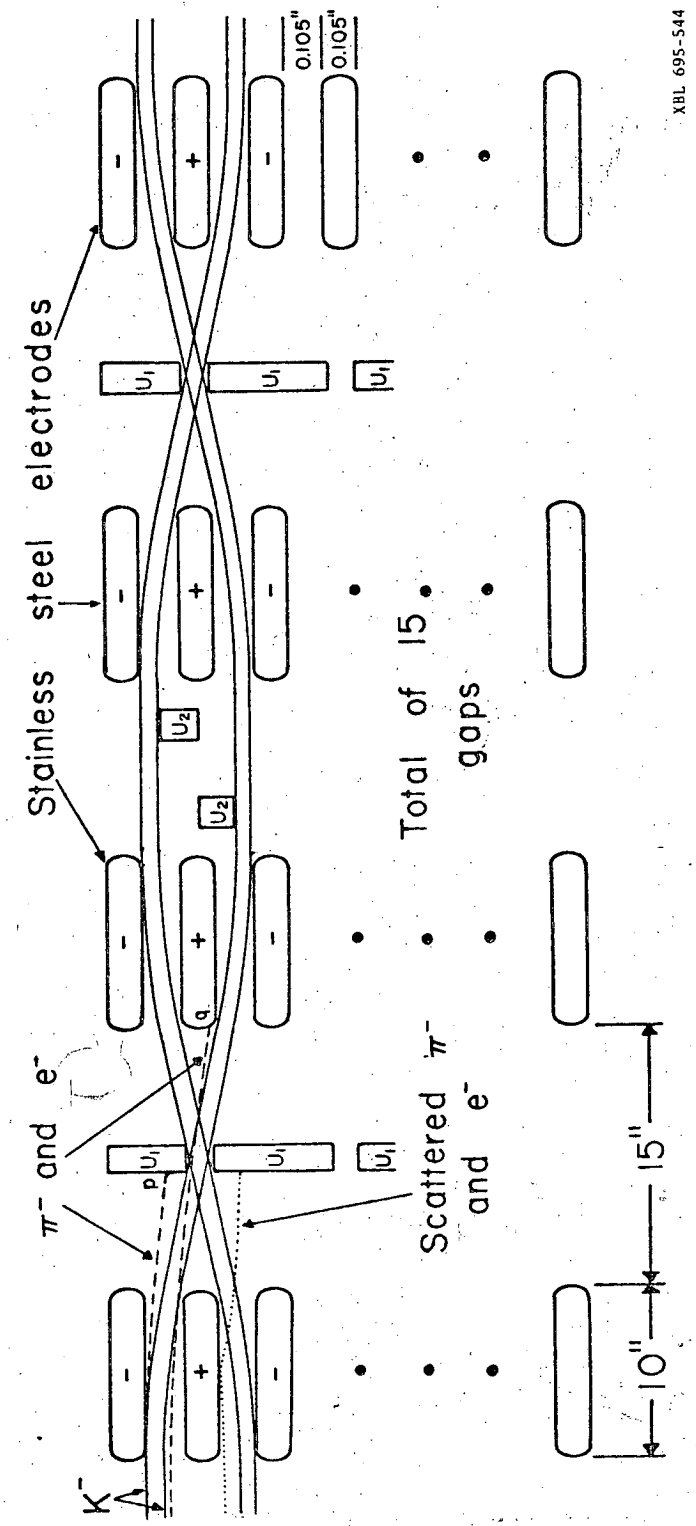

Fig. 2. Diagram of septum separator.

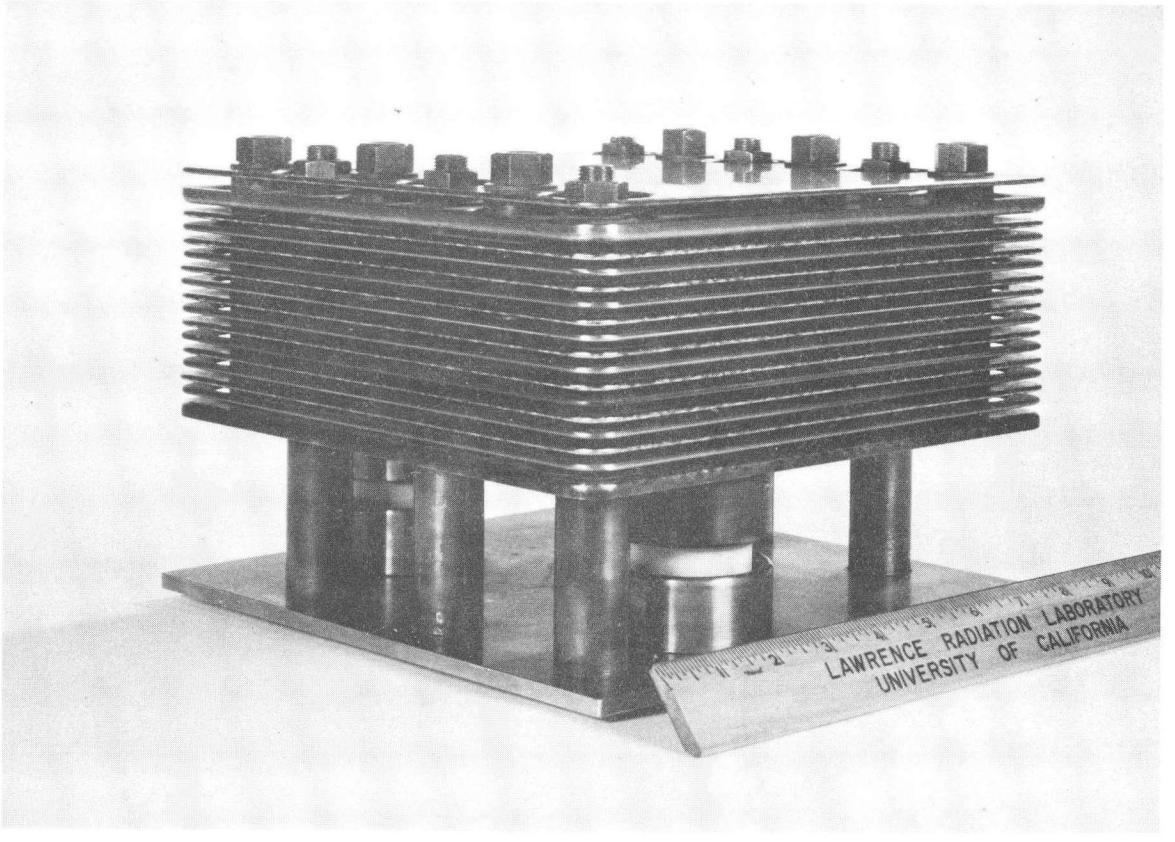

XBB 695-3010

Fig. 3. Photograph of one of the four sets of stainless steel electrodes used in the septum separator.

.050 inches is 1/4 of the thickness of a gap-electrode combination.

In contrast to conventional separators, another peculiar characteristic of the septum separator is the fact that the high voltage is not critical. Satisfactory transmission and separation is achieved within ± 2% of nominal. Figure 4 illustrates this.

C. Beam Optics

Since it requires a 4 or 5% momentum spread to get adequate K^- flux, it would be desirable to have a position-momentum correlation at the bubble chamber. Optimizing this correlation was one of the major criteria used in designing the beam optics.

Figure 5 shows the optical system used. The target is a piece of phosphor bronze 4 x 1/8 x 1/16 inches. The magnet VS1 is a small hand-wound vertical steering magnet which allows one to control the angle at which the particles enter the separator and thus allows one to satisfy the .625 mr criterion discussed above. Quadrupoles Q_1 and Q_2 are adjusted to make the beam parallel vertically and to bring it to a horizontal focus at F_{h1}. The focus at F_{h1} gives a position-momentum correlation and the momentum acceptance can thus be adjusted by changing the width of collimator 2. This focus is also important to keep the beam together horizontally, since it tends to spread owing to the dispersion in the Bevatron field. The field gradients of quadrupoles Q_3 and Q_4 and the focal effects of M* are chosen such that the beam focuses

---

*The focal effects of M are adjusted by installing iron shims on the pole pieces.

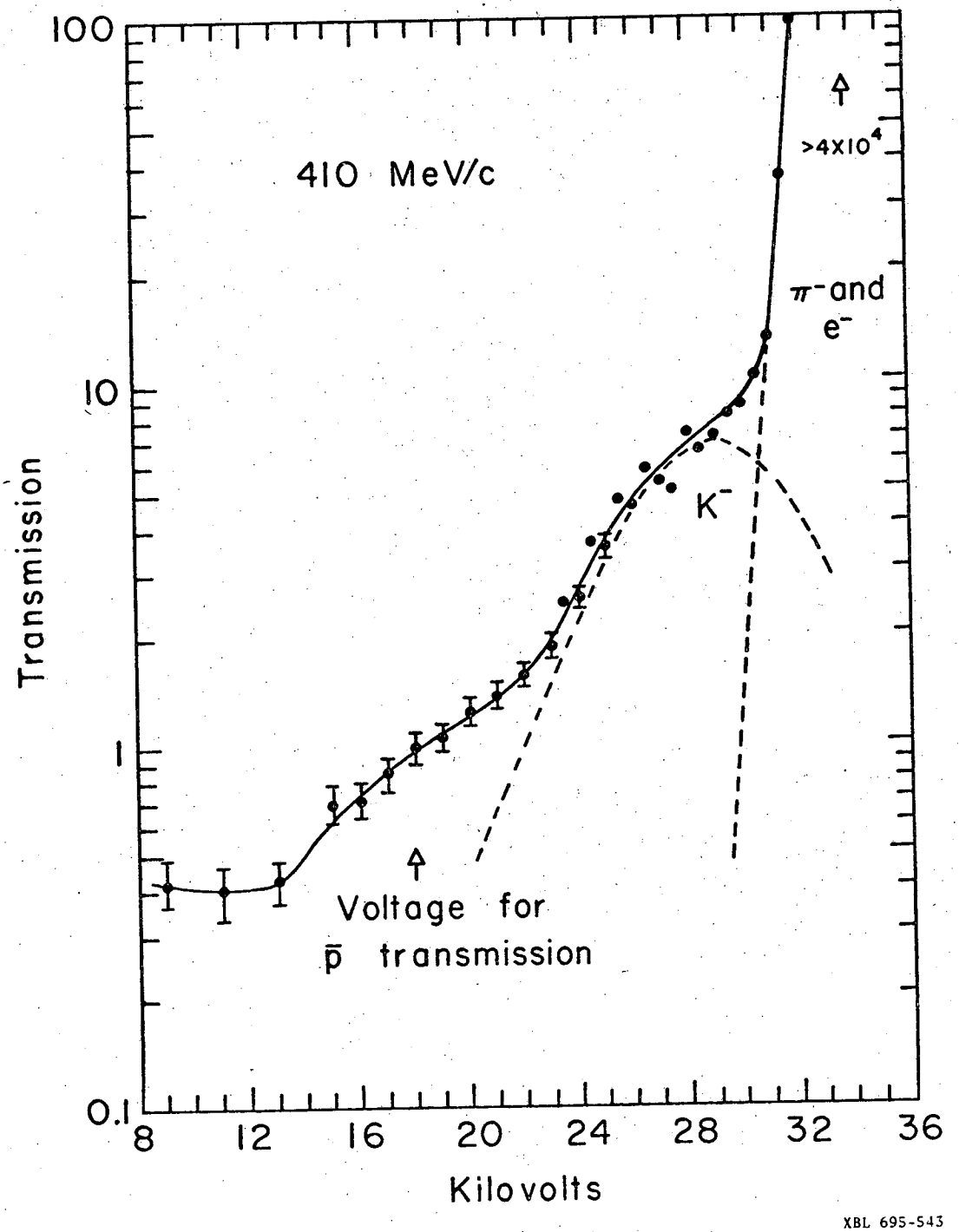

XBL 695-543

Fig. 4. Relative transmission of septum separator as a function of voltage at 410 MeV/c. The dashed lines are an estimated decomposition into the different components of the beam. There is a suggestion of a $\bar{p}$ peak at 18 kilovolts which is the proper voltage for $\bar{p}$ transmission. Measurements with the bubble chamber indicate that the $\bar{p}$ flux is roughly two orders of magnitude lower than the K^- flux.

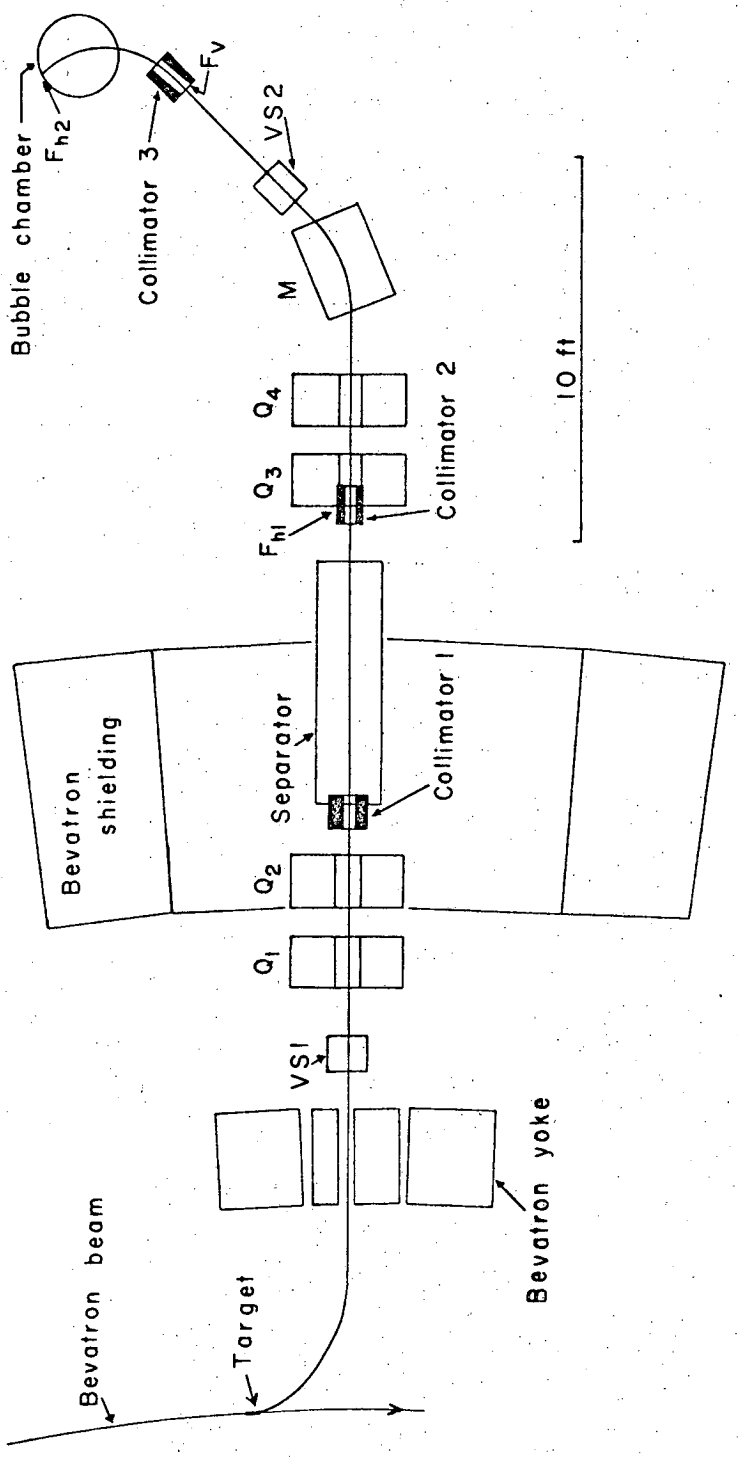

Fig. 5. Diagram of the beam-transport system. Primary momentum analysis of the beam is performed by the magnetic field of the Bevatron.

vertically at F_v (at the front edge of collimator 3) and horizontally in the neighborhood of F_{h2}. We have also adjusted Q_3, Q_4, and M to give the desired (actually the best possible in view of the constraints) position-momentum correlation at the bubble chamber. Of course the primary purpose of M is momentum analysis; the background which is degraded in momentum in the separator is swept aside by M. Magnet VS 2 allows us to steer vertically so that the K^- beam passes through collimator 3 which measures only 1/4 inch vertically.

Several special problems were encountered. As explained above it was necessary to have the beam parallel vertically to less than .625 mr. It was found that bad aberrations in the fringe field of the Bevatron made this impossible. As a consequence the beam exit pipe through the Bevatron magnet yokes was shielded with an iron pipe of 3/8-inch wall thickness. This decreases the acceptance of the system and increases the number of protons required for a given K^- flux.

The position-momentum correlation was somewhat worse than desired. It was hoped that we would be able to establish momentum to about $\pm$ 1/2%, but unavoidable effects such as finite target size and physical constraints on bubble chamber location resulted in a compromise of this goal to slightly more than $\pm$ 1% under optimum conditions.

The total performance of the beam was satisfactory. The K^--to-background ratio was roughly 3:1. Figure 6 is a typical photograph showing Σ production and decay.

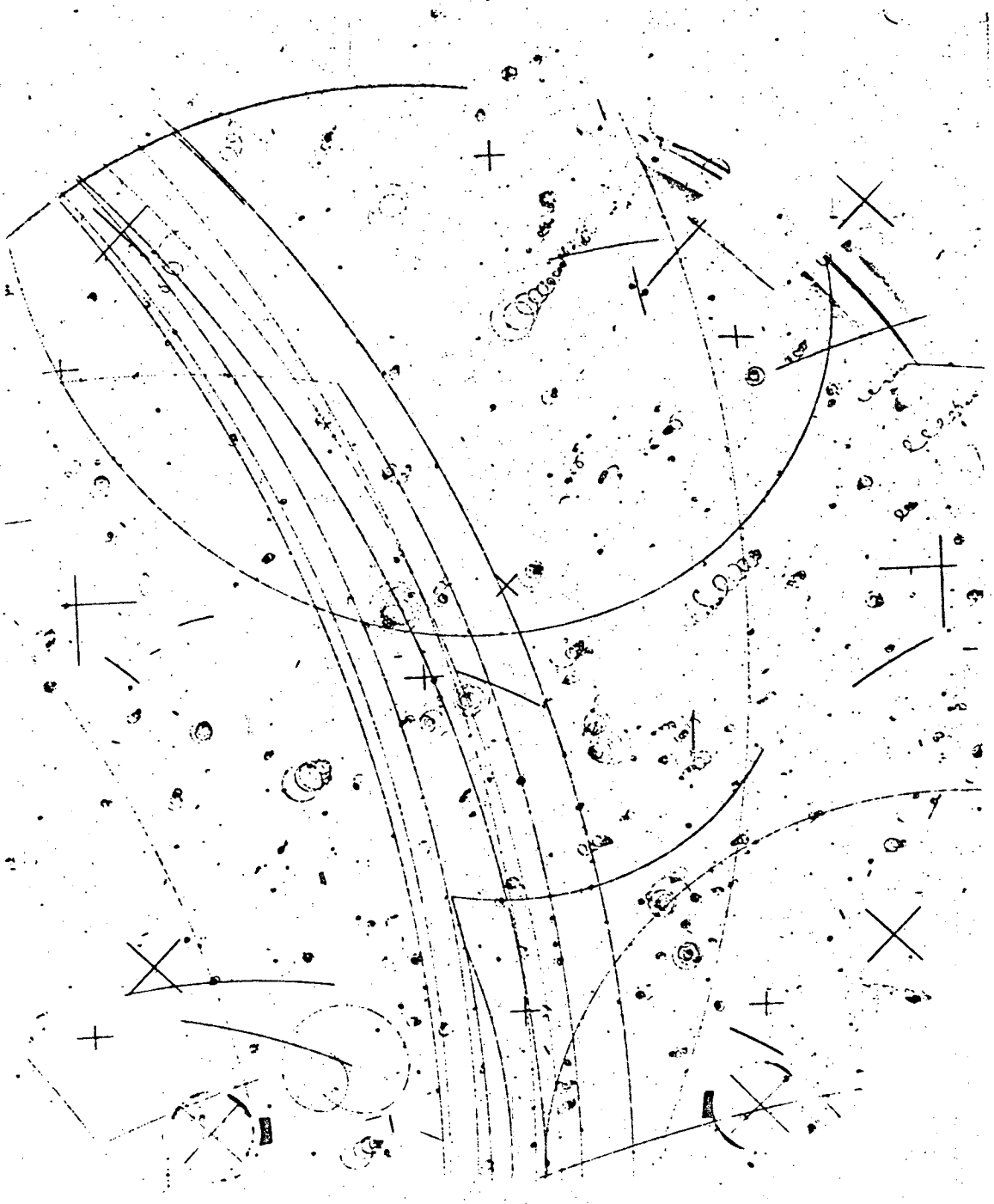

Fig. 6. Typical bubble chamber photograph showing Σ production and decay.

III. DETERMINATION OF P_Σ

As noted above, Watson, Ferro-Luzzi and Tripp have shown that the Σ's produced by the K^-p interaction around 390 MeV/c are highly polarized. The polarization is primarily due to the interference of the resonant $D_{3/2}$ ($Y_o^*(1520)$) amplitude with the large nonresonant s wave. Reliable determination of the polarization is the most critical aspect of our experiment.

Since α_o is nearly -1, the Σ^+ polarization is readily measurable through the up-down asymmetry given by (4). In contrast α_- is very small and the Σ^- polarization cannot be measured well, but must be calculated using a model of the production process. In this sense the polarizations for Σ^+ are considerably less model-dependent than those for Σ^-. Nevertheless in both cases an accurate determination of the production amplitudes is essential. In order to establish these amplitudes, we have performed a preliminary multi-channel partial-wave analysis with about 140 000 charged Σ events. The K^- momentum distributions for these events are shown in Figure 7. The polarizations obtained from our analysis are shown in Figure 8. The sign convention is such that

$$\vec{P}_\Sigma = P_\Sigma(\hat{K} \times \hat{\pi})/|\hat{K} \times \hat{\pi}| \qquad (6)$$

where $\hat{K}$ and $\hat{\pi}$ are along the incident K^- and the production π. The measured points $-\alpha_o P_\Sigma$ (we discuss these in Section IV) are shown superimposed on the curves of Figure 8a. It is evident that α_o is nearly equal to -1, that the fits are good, and that the Σ^+ polarization is well determined, particularly in the neighborhood of 385 MeV/c where

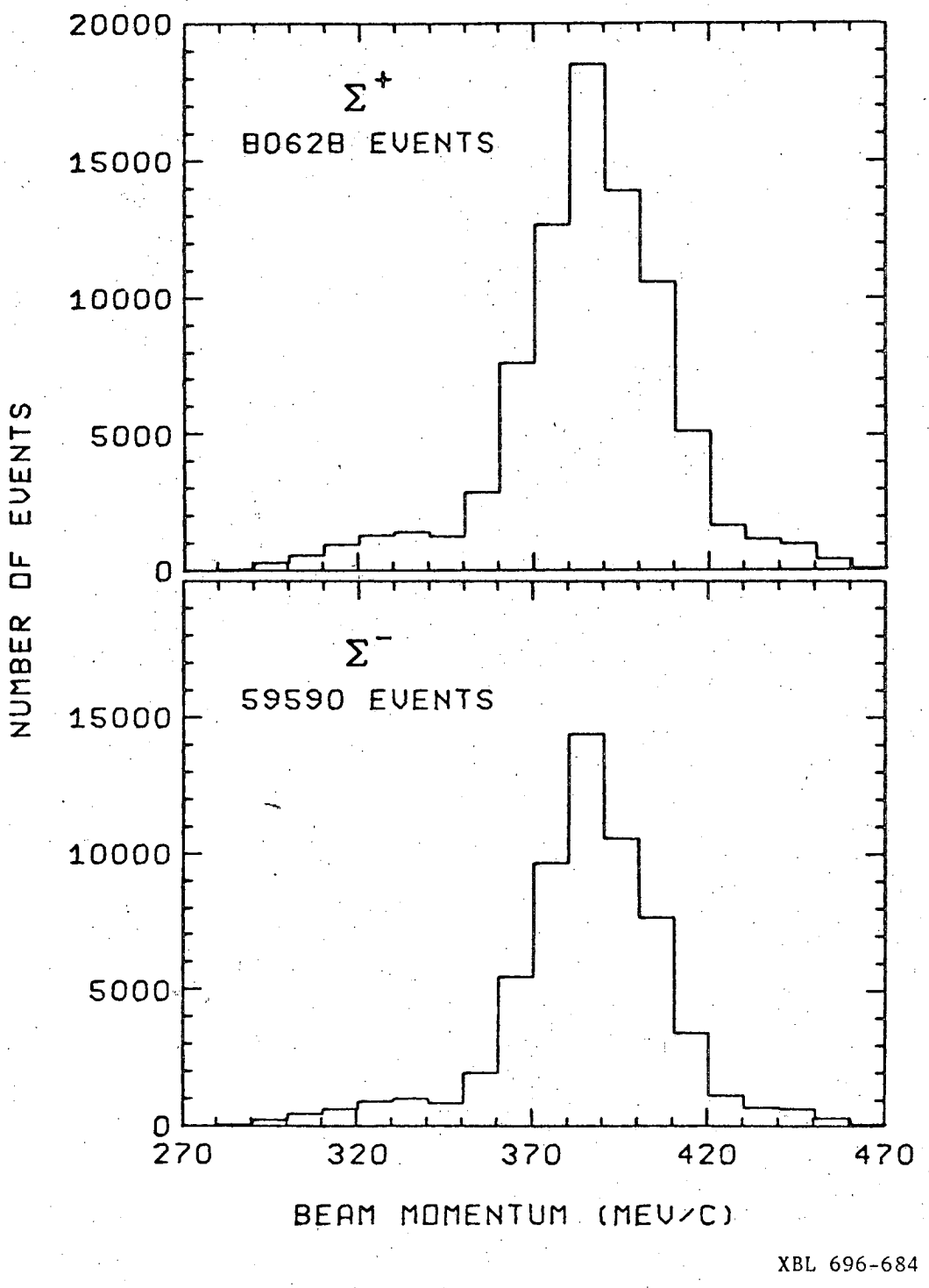

Fig. 7. Distributions of beam momentum.

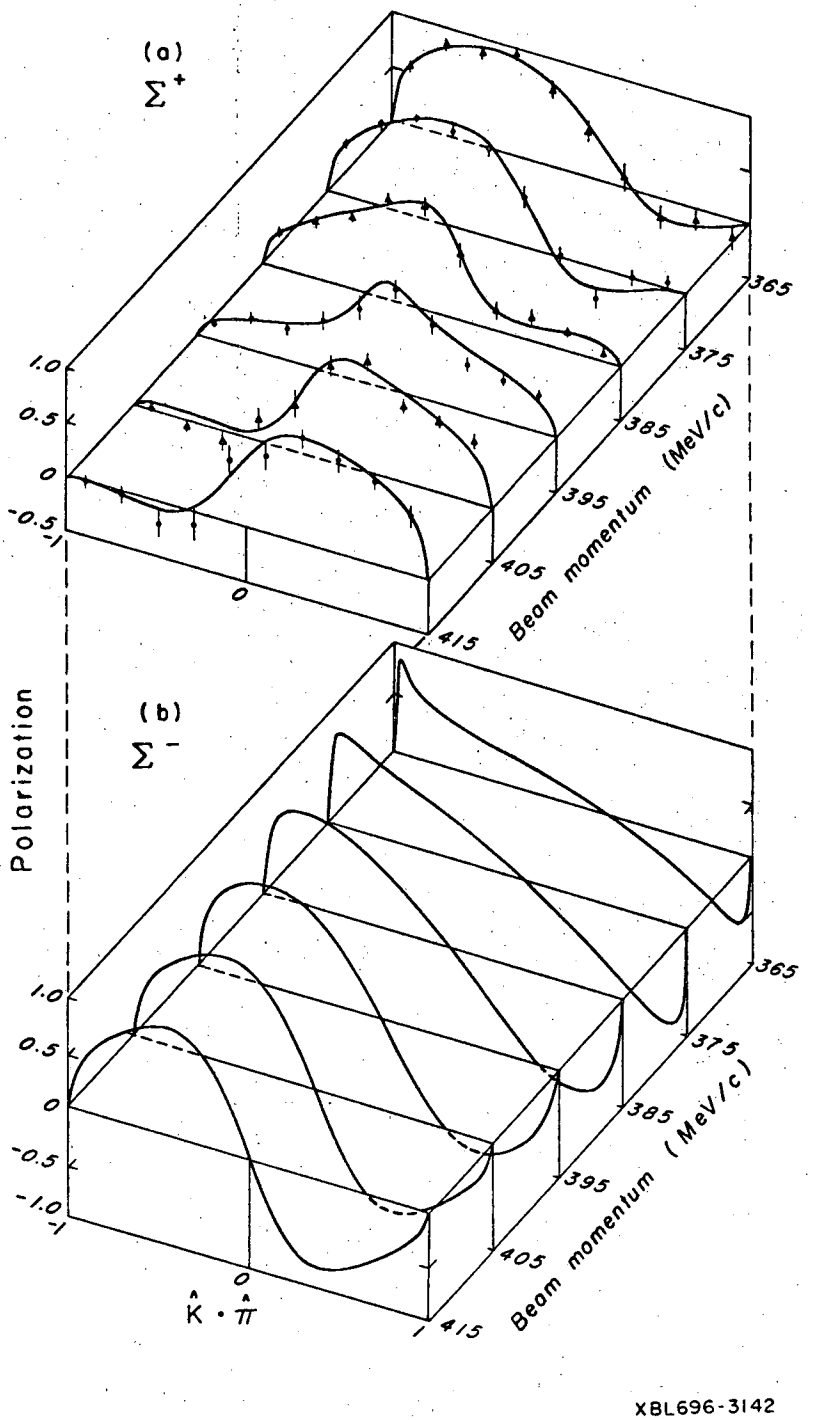

Fig. 8. Polarizations calculated from the partial wave analysis. The data points are $-\alpha_o P_{\Sigma^+}$.

the vast majority of events lie.

It is also possible to crudely confirm the calculated Σ^- polarizations in conjunction with the measurements of α_- and Φ_-. We discuss this in Sections IV and V.

We emphasize that despite the lack of any dynamical theory of the strong interactions the calculated polarizations should be quite reliable. The major assumptions are unitarity, isospin conservation, a Breit-Wigner form for the resonant amplitude, and smooth energy dependence for the nonresonant amplitudes. Furthermore the momentum is low so only a few partial waves are significant. The resonant amplitude interferes with the nonresonant amplitudes in such a way as to produce spectacularly rapid variations in the angular distributions. This condition allows a precise determination of the parameters of the resonance.

We have fitted our data to two different models consistent with the above assumptions: (a) that used by Watson, Ferro-Luzzi, and Tripp which parameterizes the nonresonant amplitudes in terms of constant scattering lengths and (b) the K matrix formalism of Ross and Shaw[6] as used for example by Kim.[7] The two models give very similar results for the calculated polarizations. For our analysis we use the values given by the K matrix formalism.

The model-dependent uncertainties in the polarizations are almost certainly smaller than the statistical uncertainty in our measurement of Φ. However the statistical uncertainties in our measurements of α are sufficiently small that we have limited the analysis to the momentum region between 360 and 420 MeV/c, thereby considerably lessening the model-dependent nature of the parameterization.

IV. MEASUREMENT OF THE α PARAMETERS

There are two principal problems involved in the determination of the α parameters. The first results from possible biases introduced in scanning and measuring the data and the second results from contamination of the true sample of events by events having similar topology. We discuss scanning and measuring biases in Section IV-A, contamination in IV-B, and the actual determination of the α parameters in IV-C.

A. Scanning and Measuring Biases

Each of the 1.3×10^6 bubble chamber expansions of our experiment was photographed from three angles. All three views are used for both scanning and measuring. The location of the three cameras relative to the bubble chamber is shown in Figure 9. The beam enters parallel to the x-y plane and is oriented approximately along the y-axis as is shown in Figure 6. The magnetic field (~ 19 kilogauss) of the bubble chamber is parallel to the z-axis.

About 30% of our film has been scanned twice. Comparison of the first and second scans gives a scanning efficiency of roughly 85%, (somewhat less for $\Sigma^+ \to \pi^o p$). Altogether the scanners have found 72 000 examples of the reactions $K^- p \to \Sigma^- \pi^+$; $\Sigma^- \to \pi^- n$ (Σ_-^-), 48 000 examples of $K^- p \to \Sigma^+ \pi^-$; $\Sigma^+ \to \pi^o p$ (Σ_o^+), and 55 000 examples of $Kp \to \Sigma^+ \pi^-$; $\Sigma^+ \to \pi^+ n$ (Σ_+^+).

These events have been measured on the Spiral Reader and Franckenstein measuring machines. Geometrical reconstruction and kinematical fitting are performed using TVGP[8] and SQUAW[9], the standard programs in use by the Alvarez group. Our Σ events have been remeasured until less

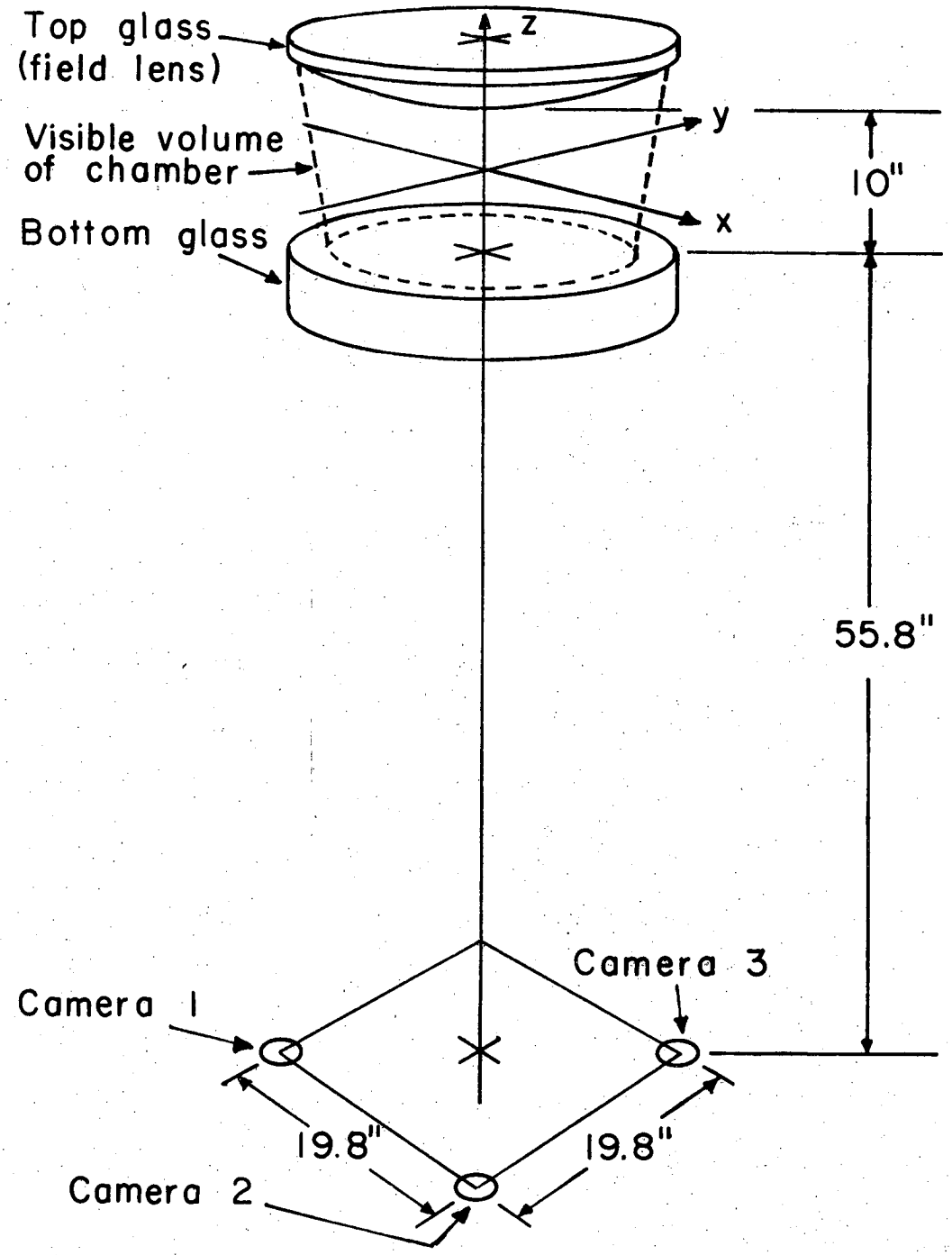

Fig. 9. Diagram of the 25-inch bubble chamber showing the location of the cameras.

than 2% fail kinematical analysis.

Since our detection efficiency (combined scanning and measuring efficiency) is less than 100%, equation (4) does not represent the observed distribution of events and may require alteration to give an unbiased estimate of α.

In general the detection efficiency e could be a function of a large number of parameters such as the lengths of all tracks, the angles between tracks, and the position of the event in the bubble chamber. For our purposes we find it convenient to represent e as a function of the azimuthal production angle of the Σ relative to the beam direction φ_p, $\cos\theta = \vec{P}_\Sigma \cdot \hat{q}$, and a set of parameters y representing all other relevant variables. The angle φ_p is defined such that $\varphi_p = 0$ when the Σ is produced in the x-y plane moving to the right of the beam direction. Quantitatively φ_p is given by

$$\varphi_p = \sin^{-1}\left[(\hat{K} \times \hat{Z}) \cdot (\hat{K} \times \hat{\Sigma})/(|\hat{K} \times \hat{Z}|\ |\hat{K} \times \hat{\Sigma}|) \right]$$

where the notation is self-explanatory, the observed distribution of events in $\cos\theta$ is given by

$$I'(\alpha P_\Sigma, \cos\theta) = \frac{(1+\alpha P_\Sigma \cos\theta)\int e(\cos\theta,\varphi_p,y)Q(y)R(\varphi_p)d\varphi_p dy}{\int(1+\alpha P_\Sigma\cos\theta)e(\cos\theta,\varphi_p,y)Q(y)R(\varphi_p)d\varphi_p dy\ d(\cos\theta)}$$

where $Q(y)$ is the probability density of the total unbiased sample of events in the parameters y, and $R(\varphi_p)$ is the probability density of the sample in φ_p. Since all values of φ_p are equally likely $R(\varphi_p) = 1$ and I' may be written as

$$I'(\alpha P_\Sigma, \cos\theta) = (1+\alpha P_\Sigma \cos\theta)\, N(\cos\theta)/D(\alpha P_\Sigma)$$

where

$$N(\cos\theta) = \int e(\cos\theta, \varphi_p, y)\, Q(y) d\varphi_p dy$$

and

$$D(\alpha P_\Sigma) = \int (1+\alpha P_\Sigma \cos\theta) e(\cos\theta, \varphi_p, y)\, Q(y) d\varphi_p dy\, d(\cos\theta) .$$

Because of the location of the cameras, the detection efficiency, to a very good approximation, must be dependent only on the projection of the event onto the x-y plane of Figure 9. Any event has a projection identical to the projection of its mirror image in the x-y plane so that under such a reflection e is unchanged. This is expressed by the equation

$$e(-\cos\theta, -\varphi_p, y) = e(\cos\theta, \varphi_p, y) \quad . \tag{7}$$

By making the substitutions $\cos\theta \to -\cos\theta$ and $\varphi_p \to -\varphi_p$ one can easily show that

$$\int \cos\theta\; e(\cos\theta, \varphi_p, y) d\varphi_p d(\cos\theta) = 0$$

so that D is independent of αP_Σ. Similarly one can show that $N(-\cos\theta) = N(\cos\theta)$ so that I' may be written as

$$I'(\alpha P_\Sigma, \cos\theta) = (1+\alpha P_\Sigma \cos\theta)\, f(\cos\theta) \tag{8}$$

where $f(\cos\theta) = N(\cos\theta)/D$ is an even function of $\cos\theta$. We emphasize that the only assumption in the derivation of (8) is the equality of e for an event and its mirror image in the x-y plane. Examination of Figure 9 shows that this condition may not be adequately satisfied

for events occurring close to the edges of the visible volume of the bubble chamber since tracks inclined upward may be slightly longer than tracks having an equal downward inclination. To minimize these edge effects, we have adopted a fiducial volume that excludes those events occurring within 6 cm of the edges of the visible volume of the bubble chamber.

One also expects the detection efficiency for an event to be nearly equal to that of its mirror image in that plane which contains the beam track and is perpendicular to the x-y plane. Under this reflection all projected lengths are unchanged as are the magnitudes of the projected angles. This is illustrated by Figure 10a and 10b and is expressed by

$$e(-\cos\theta,\ \pi-\varphi_p,y) = e(\cos\theta,\ \varphi_p,y) \qquad (9)$$

where y is now allowed to specify somewhat fewer parameters than was the case in equation (7). Condition (9) also leads to result (8).

If both (7) and (9) are satisfied it follows that

$$e(\cos\theta,\ \varphi_p + \pi,y) = e(\cos\theta,\ \varphi_p,\ y)\ . \qquad (10)$$

This simply expresses the fact that the detection efficiency is unchanged under a rotation of π about the beam direction. Equation (10) is sufficient to provide some information about the observed distribution of φ_p. This distribution is given by

$$R'(\varphi_p) = \tfrac{1}{2}\int (1+\alpha P_\Sigma \cos\theta)e(\cos\theta,\varphi_p,y)Q(y)dy\ d(\cos\theta)\ .$$

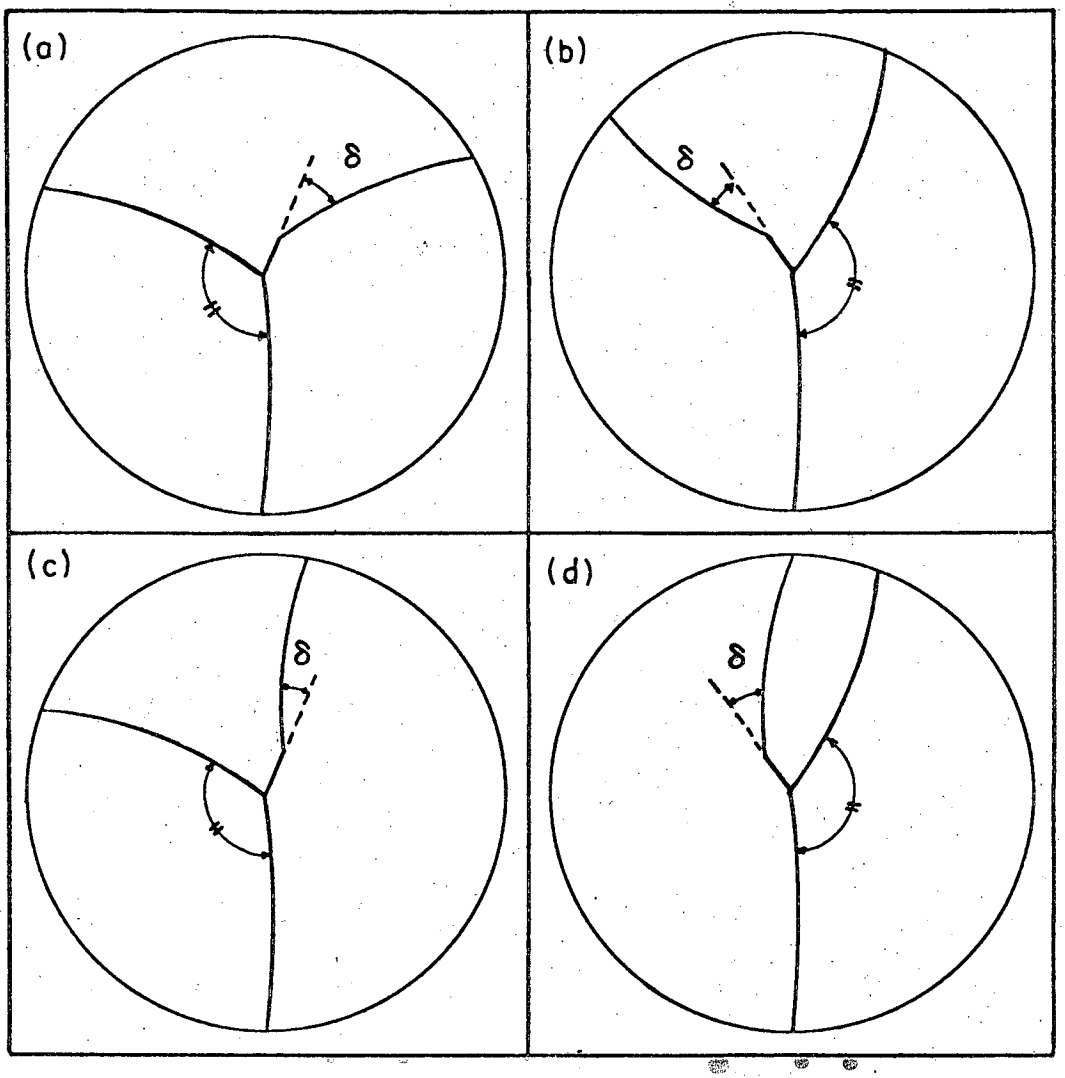

XBL 696-679

Fig. 10. Event configurations expected to have nearly equal detection efficiencies.

From (10) it follows immediately that

$$R'(\varphi_p) = R'(\varphi_p + \pi)\,. \tag{11}$$

This distribution is shown in Figure 11 for all three event types. Note that (11) implies that the number of events in which the Σ goes up (n_u) should be equal to the number of events in which the Σ goes down (n_d). Similarly the number of events in which the Σ goes to the right (n_r) should be equal to the number of events in which the Σ goes to the left (n_ℓ).

In analogy with φ_p we can define an azimuthal decay angle φ_d given by

$$\varphi_d = \sin^{-1}\left[\,(\hat{\Sigma} \times \hat{Z}) \cdot (\hat{\Sigma} \times \hat{v})/(\,|\hat{\Sigma} \times \hat{Z}|\;\;|\hat{\Sigma} \times \hat{v}|\,)\,\right]$$

where $\hat{v}$ is along the direction of the visible decay product. Equation (10) may now be rewritten as

$$e(\varphi_d + \pi,\ \varphi_p + \pi, y) = e(\varphi_d,\ \varphi_p, y).$$

It then follows that equation (11) and the subsequent statements about the up-down and left-right symmetries of φ_p are also applicable to φ_d. The distributions of φ_d are shown in Figure 12. The quantities $(n_u - n_d)/(n_u + n_d)$ and $(n_\ell - n_r)/(n_\ell + n_r)$ for both production and decay vertices are given in Table II.

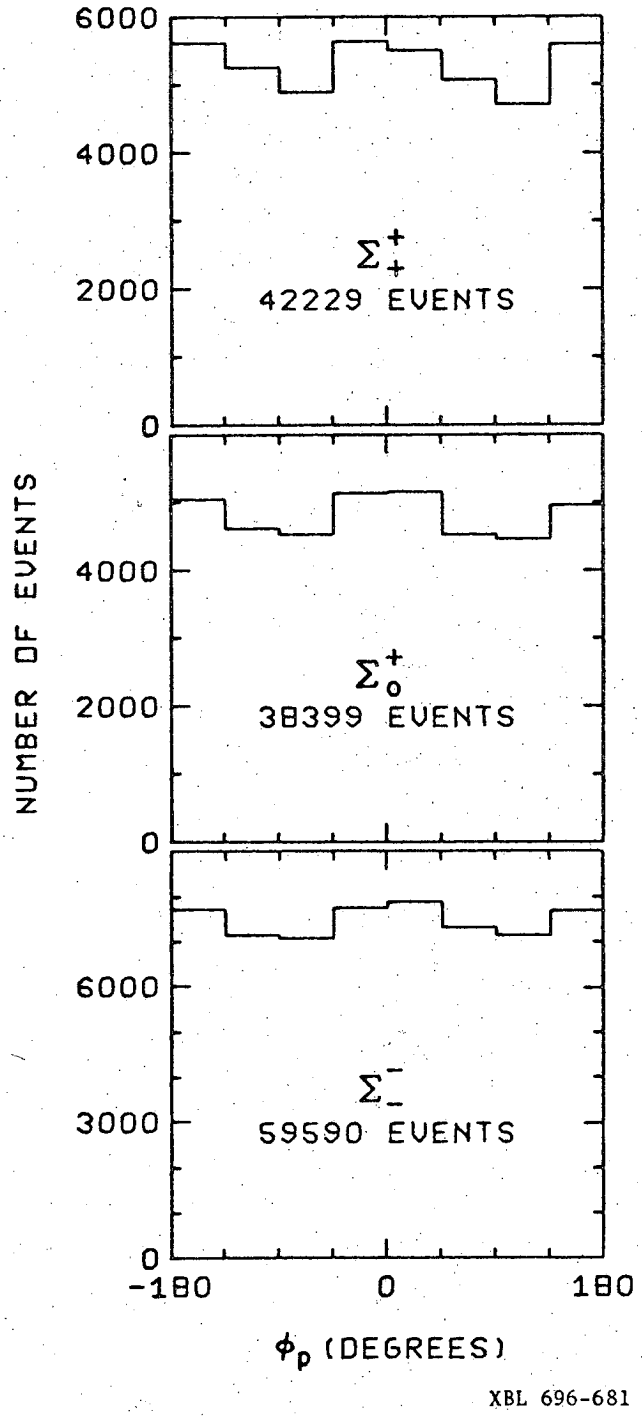

Fig. 11. Distributions of φ_p.

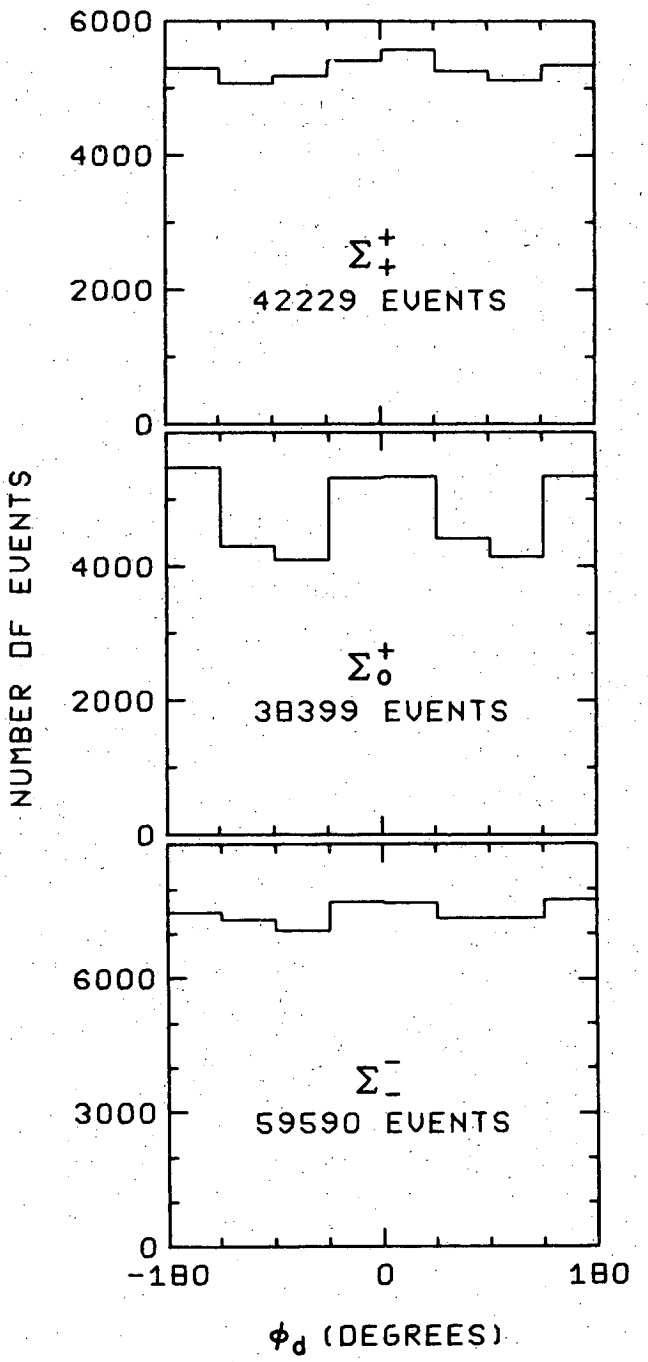

Fig. 12. Distributions of φ_d.

Table II.

	Event Type	$(n_u - n_d)/(n_u + n_d)$	$(n_\ell - n_r)/(n_\ell + n_r)$
Production Vertex	Σ^-	.0052 ± .0041	-.0058 ± .0041
	Σ^+_o	-.0071 ± .0051	-.0070 ± .0051
	Σ^+_+	-.0112 ± .0049	.0012 ± .0049
	Total	-.0031 ± .0027	-.0040 ± .0027
Decay Vertex	Σ^-	.0101 ± .0041	.0014 ± .0041
	Σ^+_o	.0014 ± .0051	.0031 ± .0051
	Σ^+_+	.0084 ± .0049	-.0136 ± .0049
	Total	.0072 ± .0027	-.0027 ± .0027

In addition to the symmetries discussed above, one also expects the configurations shown in Figures 10c and 10d to have detection efficiencies roughly equal to those of the configurations of Figures 10a and 10b. These additional equalities explain the approximate 4-fold symmetry exhibited by the distributions of φ_p and φ_d. As expected the minima in these distributions occur when the production or decay plane is parallel to the camera axes.

For an unbiased sample, $\hat{\Sigma} \cdot \hat{v}$ as evaluated in the Σ rest frame should be uniformly distributed between -1 and 1. The experimental distributions are shown in Figure 13. Depletion occurs for $\hat{\Sigma} \cdot \hat{v} \approx 1$ (and also $\hat{\Sigma} \cdot \hat{v} \approx -1$ in the case of Σ^+_o). This corresponds to small values of the angle δ in Figure 10. Such Σ decays are clearly difficult to detect. The situation is much worse for the Σ^+_o decay

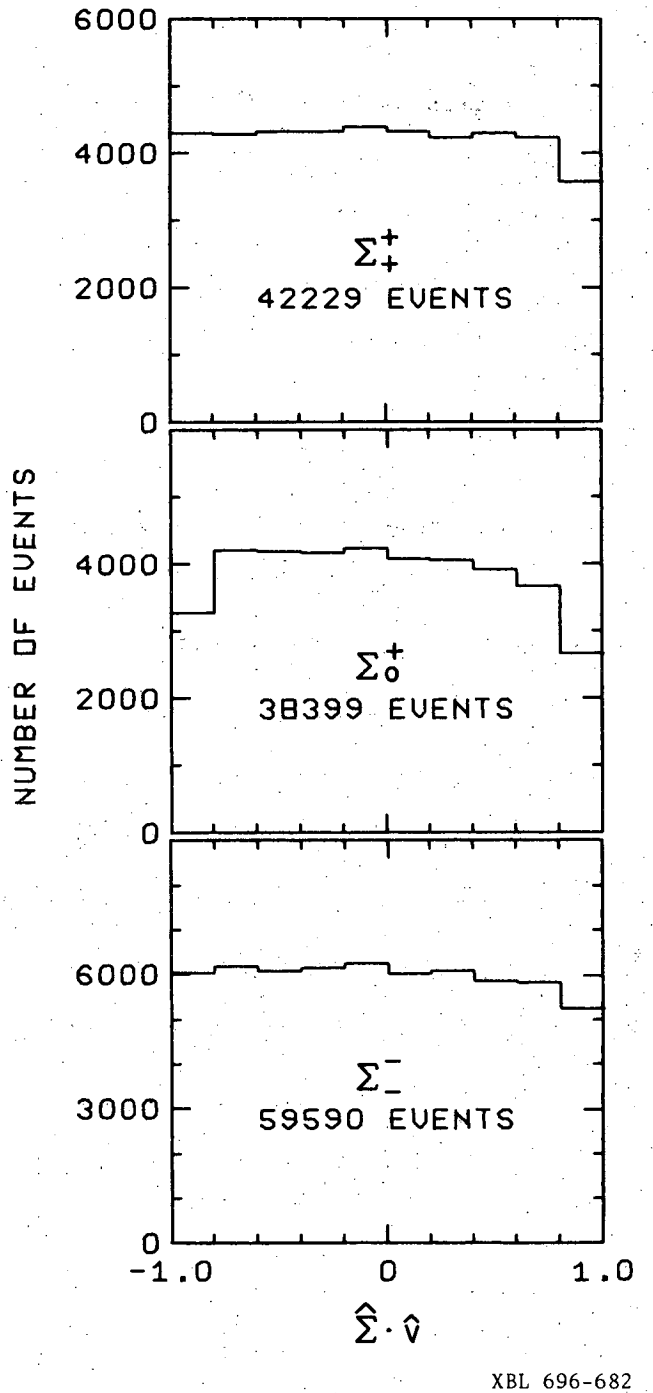

Fig. 13. Distributions of $\hat{\Sigma} \cdot \hat{v}$.

since a given laboratory angle corresponds to a larger center-of-mass angle than is the case for the Σ^-_- and Σ^+_+ decay modes. Furthermore, the ionization of a Σ and proton are more nearly equal than the ionization of a Σ and a pion so that track darkness cannot be used to identify the decay vertex.

Fortunately those decays for which $\hat{\Sigma} \cdot \hat{v} \approx \pm 1$ must have small values of $\vec{P_\Sigma} \cdot \hat{q}$ and therefore contribute very little to the measurement of α.

In conclusion, the total detection losses are small ($\sim$ 15%) and are particularly small for those events which contribute most heavily to the measurement of α. It is a priori extremely unlikely that the losses that do occur could in any way bias α, and the distributions of φ_p and φ_d are consistent with this expectation.

B. Contamination of Sample

There are two types of contamination in our data. The first type results from non-sigma events which are topologically similar to the true events. The second type is far more serious and results from ambiguities between Σ^+_o and Σ^+_+ events.

A Σ^+_o event may be simulated by the sequence of reactions $K^-p \to K^-p$; $pp \to pp$, where one of the scattered protons is too short to be visible. Since the ionization of the K^- is typically several times that of a π^-, most of these K^-p events can be properly identified by the scanners. Also, the two-event types are kinematically rather different.

All events identified as $K^-p \to K^-p$ by the scanners have been fitted

to both $K^-p \to K^-p$ and the Σ_o^+ hypothesis with zero-length Σ. Of 42 000 events only 1600 give acceptable fits to Σ_o^+. Closer examination shows that roughly 1200 of these are Σ_o^+ while 400 are K^-p scatterings. Since the visible proton loses very little energy in a small-angle pp scattering, these K^-p events are very similar to those simulating finite-length Σ events. In fact it should be somewhat more difficult to obtain an adequate fit to the finite-length Σ hypothesis because of the additional constraints imposed by measuring the fake Σ. We would thus expect that less than 1% of those K^-p scatterings called Σ_o^+ by the scanners will actually fit the Σ_o^+ hypothesis. This estimate could be somewhat low because those K^-p events that are ambiguous with Σ_o^+ have a proton momentum of about 300 MeV/c where the pp cross section is relatively high. Roughly 1% of the events called Σ_o^+ by the scanners fit only the K^-p hypothesis. Since this must represent nearly the entire sample of misassigned events, we estimate the total contamination to be about .01%. Furthermore, the small angle pp scatterings must have small values of $\vec{P}_\Sigma \cdot \hat{q}$ so that they contribute relatively little to the measurement of α. Even if our estimate of contamination is an order of magnitude low, the bias would not be serious.

The Σ^- events can be simulated by $K^-p \to K^-p$ followed by $K^- \to \mu^- \bar{\nu}$ or $K^- \to \pi^-\pi^o$. There are many such events but nearly all are rejected by the scanners. Slightly over 1% of the events called Σ^- fit only the K^-p hypothesis. Again the situation is kinematically quite unambiguous and this must represent nearly the entire sample of misidentified K^-p events. We conclude that the contamination is

considerably less than 1%. Even a contamination of 2 or 3% would be relatively innocuous since α_- as determined by the K^-p events must be zero which, according to Table I, is nearly correct.

The Σ^+_+ events should be free of non-sigma contamination.

As noted above, the most difficult contamination problem results from the ambiguity between Σ^+_o and Σ^+_+. There are three categories of information which allow us to distinguish these decay modes:

1. Kinematics

Only about 19% of all Σ^+ decays fit both Σ^+_+ and Σ^+_o.

2. Ionization Information

The momentum of the pion or proton is typically several hundred MeV/c so that the proton ionizes much more heavily than the pion. Information about the ionization is obtained in the following ways:

(a) For those events in which the charged decay product makes an angle of less than 50^o with respect to the x-y plane (dip angle λ), the scanners are able to distinguish Σ^+_+ and Σ^+_o with better than 95% reliability. All tracks having $|\lambda| > 50^o$ appear rather dark and it is more difficult to distinguish differences in ionization. The scanners are able to distinguish such tracks with better than 75% reliability.

(b) The range of a proton is much smaller than that of a pion having equal momentum and many protons stop in the bubble chamber. This stopping proton information alone is sufficient to reduce the ambiguities from 19% to 7%.

(c) The range information is also used in another way. If the fitted momentum of the proton hypothesis gives a range significantly smaller than the measured length of the track, the proton hypothesis

may be rejected.

(d) Because of its greater energy loss, the radius of curvature of a proton decreases more rapidly than that of a pion. In some cases this difference gives an unambiguous mass determination in the process of geometrical track reconstruction. In all cases, TVGP computes a track χ^2 for both mass hypotheses.

(e) About half of our events were measured on the Spiral Reader. The Spiral Reader automatically measures track darkness and this information is used to calculate a χ^2 for each mass hypothesis.

3. A Priori Probability

Although both Σ_+^+ and Σ_o^+ events are uniformly distributed in $\hat{\Sigma} \cdot \hat{v}$ in the Σ rest frame, the laboratory distributions are quite dissimilar. An a priori probability for each hypothesis may be assigned on the basis of $\hat{\Sigma} \cdot \hat{v}$ as measured in the laboratory.

Those events that are unambiguously fitted by SQUAW are checked for consistency with the range-momentum conditions of 2b and 2c. If consistent, these events are considered to be truly unambiguous.

For the ambiguous events it is desirable to obtain a number representing in some sense the simultaneous goodness of fit to all of the above categories of information. If we denote a given mass hypothesis by the discrete variable m and the kinematic variables of an event by ξ the probability density in ξ is given by

$$P(\xi ; m) \propto \frac{e^{-\frac{1}{2}\chi^2(\xi ; m)}}{\left[\det E(m) \right]^{\frac{1}{2}}}$$

where $E(m)$ is the error matrix used in constructing χ^2. The matrix E

is dependent on m because the errors assigned to the measured quantities of bubble chamber tracks are largely determined by Coulomb scattering. Given ξ we can regard $P(\xi, m)$ as a likelihood function for the determination of m. We thus interpret $P(\xi, m_\pi)/P(\xi, m_p)$ as the probability ratio for Σ_+^+ relative to Σ_o^+.

It is possible to assign a probability ratio to each of the other types of information available. The product of these ratios expresses the combined probability ratio r for the two mass hypotheses. Details of the probability assignments are given in Appendix A. In some cases rather crude estimates are employed to assign these probabilities. In any case, our goal is only to find some recipe that effectively separates the two mass hypotheses. To evaluate the effectiveness of the separation, 897 Σ_o^+ events ($r < 1$) were very carefully examined on the scanning projector. There are no cases in which definite misassignment has occurred but there are three events about which we are unable to make a meaningful decision. We also examined 1032 Σ_+^+ events ($r > 1$). Among these we find three misassigned Σ_o^+ events and seven events about which we are unable to make a decision.

Those Σ_+^+ events having values of r close to unity have about the same weight in the determination of α_+ as those with large values of r. We choose to correct α_+ for 0.3% contamination and leave α_o unchanged.

C. Measurement of α

We measure αP_Σ for all three event types by the method of moments. The first moment of equation (8) is given by

$$\langle \cos\theta \rangle = \int_{-1}^{1} \cos\theta \, (1+\alpha P_\Sigma \cos\theta) \, f(\cos\theta) \, d(\cos\theta)$$
$$= \alpha P_\Sigma \int_{-1}^{1} \cos^2\theta \, f(\cos\theta) \, d(\cos\theta) \, .$$

The second moment is given by

$$\langle \cos^2\theta \rangle = \int_{-1}^{1} \cos^2\theta (1+\alpha P_\Sigma \cos\theta) \, f(\cos\theta) \, d(\cos\theta)$$
$$= \int_{-1}^{1} \cos^2\theta \, f(\cos\theta) \, d(\cos\theta)$$

so that

$$\alpha P = \langle \cos\theta \rangle / \langle \cos^2\theta \rangle = \sum_{i=1}^{N} \cos\theta \Big/ \sum_{i=1}^{N} \cos^2\theta$$

where N is the total number of events. The statistical uncertainty in αP_Σ is given by*

$$\delta(\alpha P_\Sigma) = \left[\sum \cos^2\theta_i \, (1 - \alpha P_\Sigma \cos\theta_i)^2 \right]^{1/2} / \sum \cos^2\theta_i$$

The measured values of $\alpha_- P_\Sigma^-$ and $\alpha_o P_\Sigma^+$ are used as input data for the multi-channel partial-wave analysis described in Section III. The values of α_- and α_o are determined simultaneously with P_Σ by χ^2 minimization. This method of determining α has the virtue that statistical uncertainties in P_Σ are automatically reflected in the uncertainty assigned to α. The measured values of $-\alpha_o P_\Sigma^+$ together with the curves

---

* In performing our analysis we used an incorrect formula for calculating the uncertainty in αP_Σ. This has resulted in a negligible ($\lesssim 5\%$) overestimation of the uncertainty in α_o. We are indebted to Prof. George H. Trilling for bringing this to our attention.

of $P_{\Sigma}+$ have already been shown in Figure 8a. The measured values of $\alpha_{-}P_{\Sigma}-$ together with the fitted curves are shown in Figure 14. The values of χ^2 for both $\alpha_{-}P_{\Sigma}-$ and $\alpha_{o}P_{\Sigma}+$ are good, being 44 in both cases for 60 data points.* The values of α are

$$\alpha_{-} = -0.071 \pm 0.012 ,$$

$$\alpha_{o} = -0.999 \pm 0.022 .$$

These values are obtained from about 51 000 Σ^{-} events and 32 000 Σ^{+}_{o} events having beam momenta between 360 and 420 MeV/c.

The quoted uncertainties are statistical only, however since the partial-wave analysis is preliminary, we have examined the correlations of α_{o} with possible systematic and model-dependent biases. We believe these possible biases have less than a 1% effect on α_{o} and we neglect them. We recognize that this constitutes the weakest point of our experiment, however a more detailed partial-wave analysis is in progress and will be reported in the future.

It is possible to present the information in Figure 14 in a way that crudely confirms the calculated values of Σ^{-} polarization (P_{calc}) shown in Figure 8b.

The sample of Σ^{-} events is divided into four bins according to

---

* The number of degrees of freedom is somewhat fewer than 60 since the measured values of αP_{Σ} contribute to the determination of α and the Σ production amplitudes. For the complete partial-wave analysis, we obtain $\chi^2 = 209$ for 215 degrees of freedom.

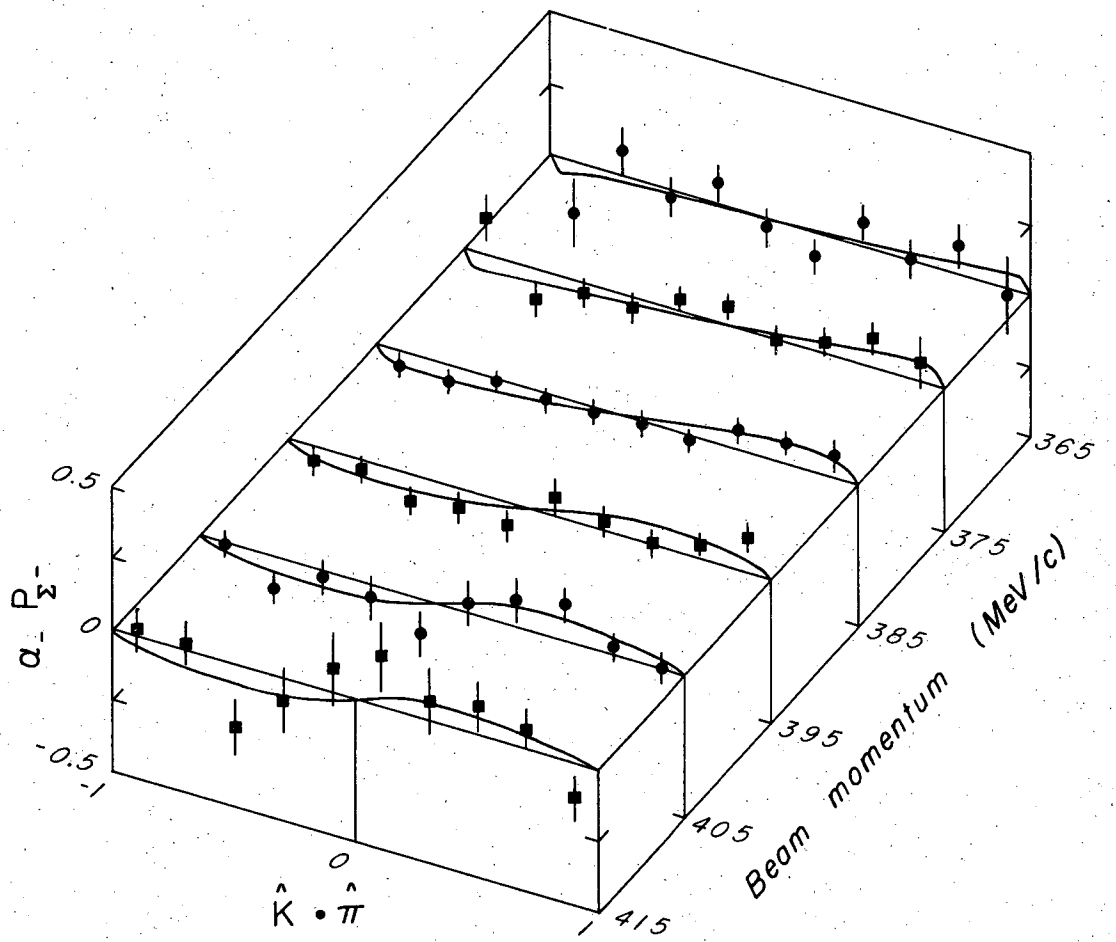

XBL 697-854

Fig. 14. Measured values of $\alpha_- P_{\Sigma^-}$ together with fitted curves.

P_{calc}. The first bin contains those events having $-1 < P_{calc} < -.5$, the second bin contains those events having $-.5 < P_{calc} < 0$, and so on. For each bin we measure $\alpha_- P_\Sigma$-. The measured values are shown in Figure 15 as a function of P_{calc}. The points have been plotted at the mean value of P_{calc} for each bin. If the calculated polarizations are correct, the measured values of $\alpha_- P_\Sigma$- should lie on a straight line with slope α. The line shown is the best least squares fit to our data and has a slope of -.076. The data clearly provide some confirmation of the gross features of the curves in Figure 8b.

In the case of α_+ we can eliminate all model dependence by measuring α_+/α_o. For this determination, we use all of our data in the momentum region from 300 to 460 MeV/c. The ratio $R = \alpha_+/\alpha_o$ is given by minimizing

$$\chi^2(R) = \sum_i \left\{ \frac{\left[R(\alpha_o P_{\Sigma^+}) - (\alpha_+ P_{\Sigma^+}) \right]^2}{\left[R\, \delta(\alpha_o P_{\Sigma^+}) \right]^2 + \left[\delta(\alpha_+ P_{\Sigma^+}) \right]^2} \right\}_i .$$

We obtain

$$\alpha_+/\alpha_o = -0.062 \pm 0.016 \ .$$

This result has been corrected for 0.3% contamination. The minimum value of χ^2 is 133 for 159 degrees of freedom. The measurement is based on 38 000 Σ^+_o events and 42 000 Σ^+_+ events.

Assuming the Σ polarizations to be known exactly, we have also measured α_- and α_+ by the method of maximum likelihood. The logarithm of the likelihood function as obtained from (8) is given by

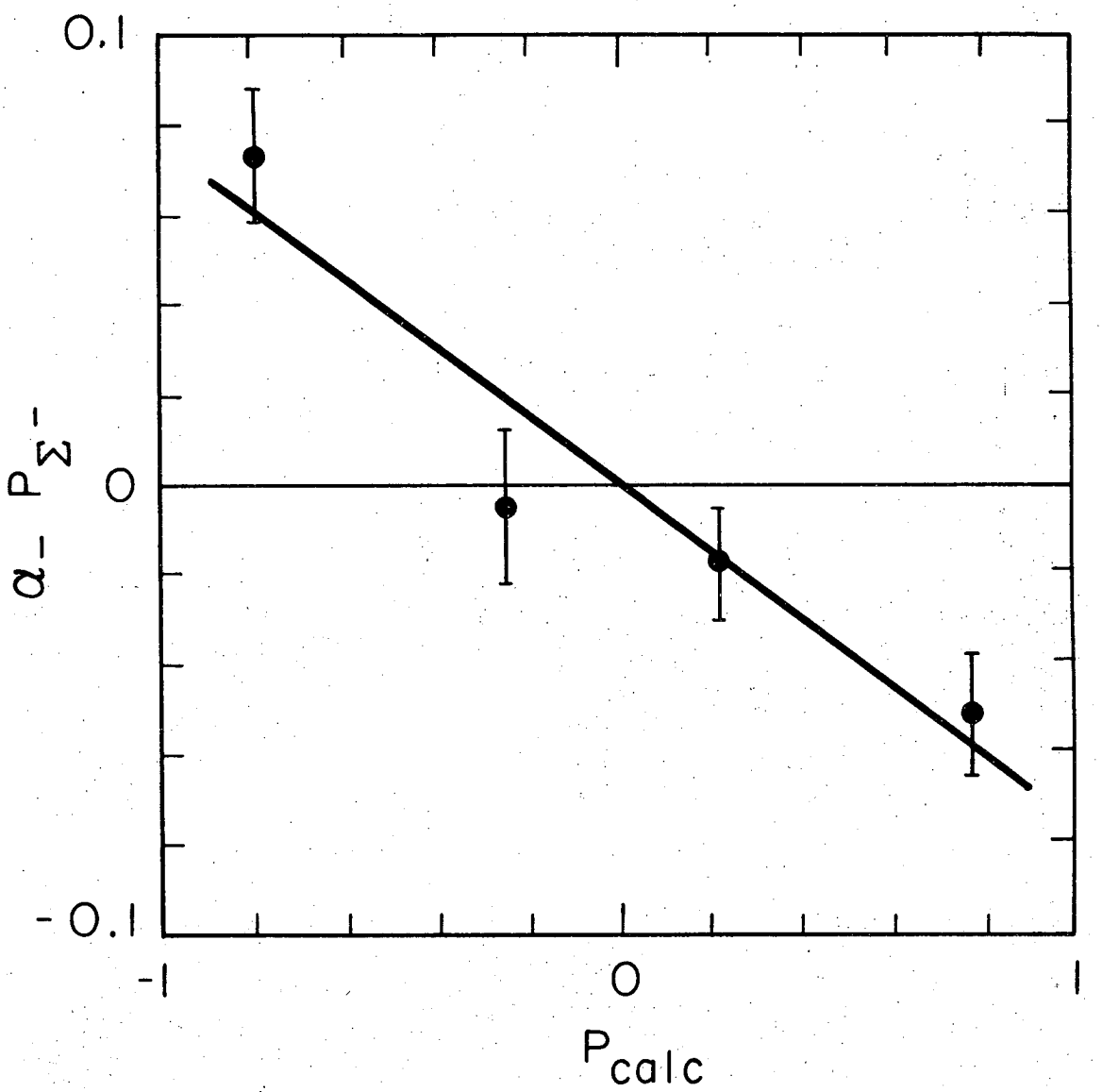

Fig. 15. Measured values of $\alpha_- P_{\Sigma^-}$ as a function of calculated Σ^- polarization.

$$\ln \mathcal{L}(\alpha) = \sum_{i=1}^{N} \ln \left[1 + \alpha \, (P_{\Sigma} \cos \theta)_i \right] .$$

The term N ln f(cos θ) has been dropped since it is independent of α. The curves of ln $\mathcal{L}(\alpha)$ are shown in Figure 16. The values of α obtained from these curves are

$$\alpha_- = -0.072 \pm 0.012$$

and

$$\alpha_+ = 0.069 \pm 0.017 \ .$$

These values of α are based on the sample of events between 360 and 420 MeV/c and again we have corrected α_+ for 0.3% contamination.

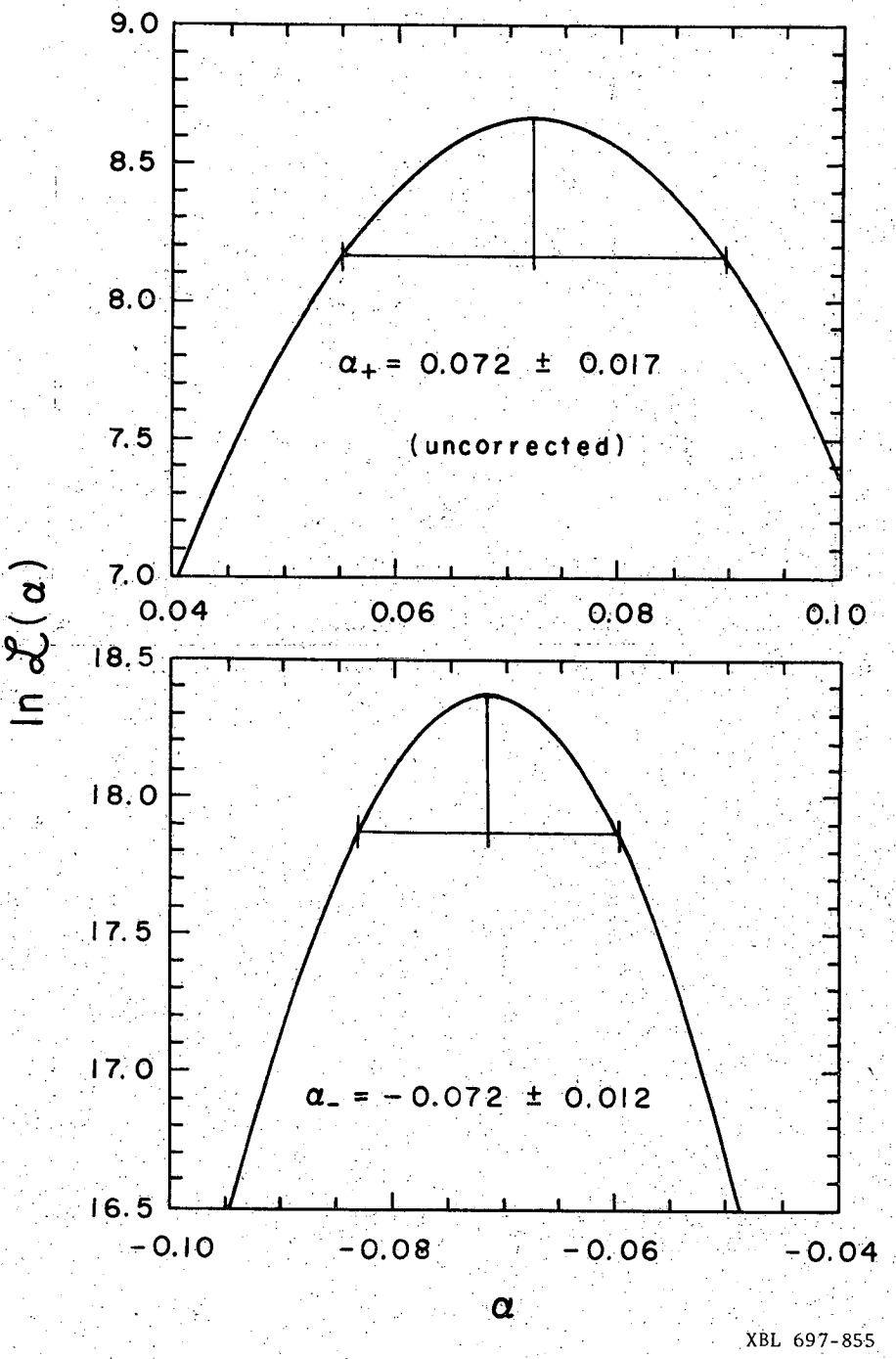

Fig. 16. Logarithm of likelihood functions used to determine α_- and α_+.

V. MEASUREMENT OF THE Φ PARAMETERS

As explained in Section I, we measure Φ by observing the angular distribution of np scatterings produced by the reactions $\Sigma^{\pm} \to \pi^{\pm} n$; $np \to np$. The probability density for the np reaction is given by

$$W(\vec{P}_n \cdot \hat{s})d\zeta = 1/2(1 + A\vec{P}_n \cdot \hat{s})d\zeta \qquad (12)$$

where $\hat{s}$ is the unit normal to the np scattering plane and A is the np scattering asymmetry. The azimuthal scattering angle ζ is given by $\zeta = \cos^{-1}(\vec{P}_n \cdot \hat{s}/|\vec{P}_n|)$. We use the values of A determined by Arndt and MacGregor.[10] These are shown in Figure 17. The vector $\vec{P}_n$ appearing in (12) is the polarization of the neutron as observed in that rest frame of the neutron obtained by a direct Lorentz transformation from the center of mass of the np system, while $\vec{P}_n$ as given by (5) is measured in that rest frame of the neutron obtained by a Lorentz transformation along $\hat{q}$ from that Σ rest frame (ΣRF) in which $\hat{q}$ and $\vec{P}_\Sigma$ are measured. The polarization $\vec{P}_\Sigma$ as given by (6) is correct in either the ΣRF obtained by a direct Lorentz transformation from the laboratory (ΣRF_{lab}) or the ΣRF obtained by a transformation from the K^-p center of mass system.

Because of the curvature of the Σ in the magnetic field of the bubble chamber ΣRF_{lab} rotates. Furthermore both $\vec{P}_\Sigma$ and $\vec{P}_n$ precess. Owing to the short Σ mean life these effects result in a negligible change in $\vec{P}_\Sigma$, but for a low momentum neutron $\vec{P}_n$ can change by more than a radian.

For simplicity in writing equations we will continue to use the nonrelativistic notation. In particular we make no distinction

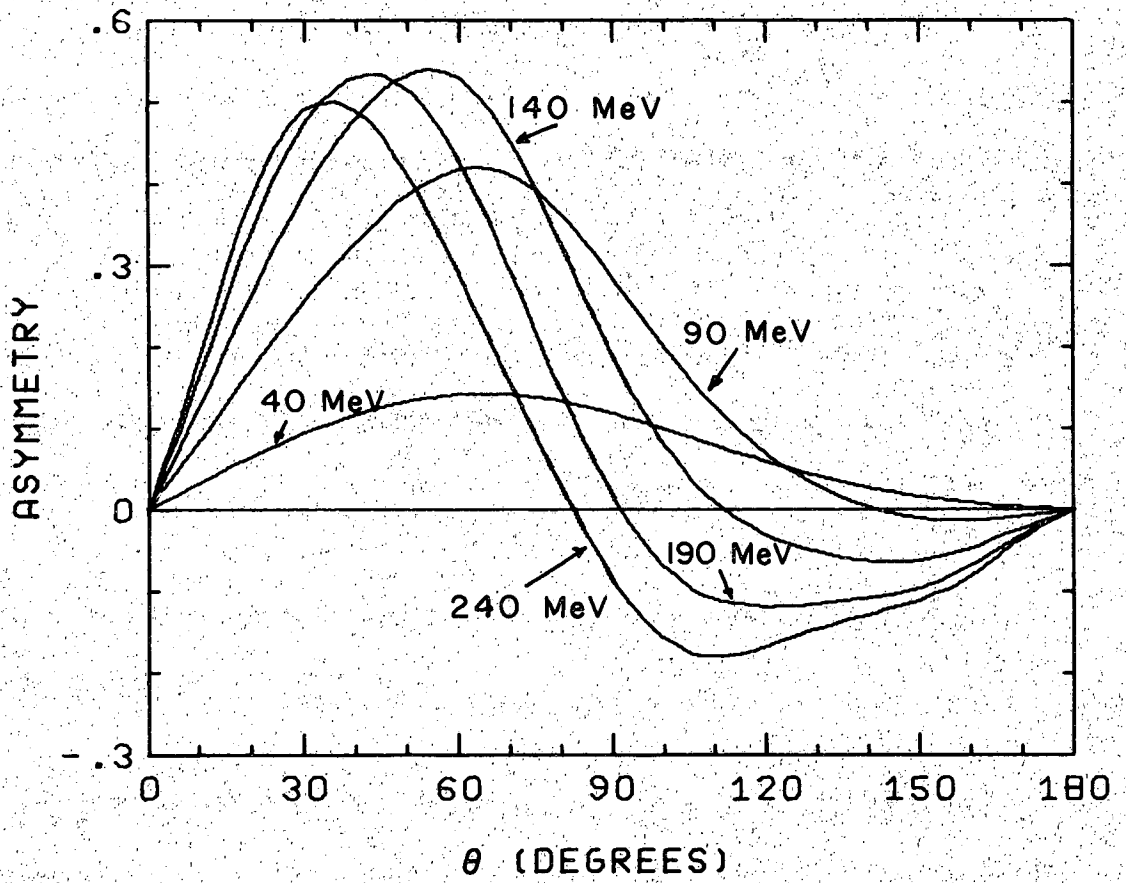

XBL 696-680

Fig. 17. Scattering asymmetry for np scattering as a function of kinetic energy and scattering angle.

between $\vec{P}_n$ in (5) and $\vec{P}_n$ in (12). However, in performing all calculations we employ the following procedure:

the polarization $\vec{P}_n$ in (5) is generalized to a 4-vector.[11] We transform this 4-vector to ΣRF_{lab} and from ΣRF_{lab} to the laboratory. In the laboratory the precession of $\vec{P}_n$ is easily calculated owing to the simple form of the electromagnetic field strength tensor. The remaining transformation to the frame appropriate to (12) is unnecessary since $\vec{P}_n \cdot \hat{s}$ would be unchanged.

A. Identification of Events

The relatively low K^- yield of the Bevatron and rapid decay of a low momentum K^- beam necessitated placing the bubble chamber very close to the Bevatron thus precluding the use of adequate shielding against background. In particular a high background flux of fast neutrons produced about 20 np scatterings per frame, making it impossible to select the real events simply by scanning.

In order to select those scatterings resulting from Σ decay, we first measured and analyzed about 20 000 events of the type $\Sigma^+ \rightarrow n\pi^+$ and 52 000 events of the type $\Sigma^- \rightarrow n\pi^-$. We rejected those events having a neutron momentum less than 275 MeV/c. At these low momenta A is very small and the events would not significantly contribute to our results. Elimination of the low momentum neutrons reduced the total sample to about 43 000 events. The results of the analysis of these 43 000 events were used to predict the direction of the neutrons on the scanning projector in three different views. We then scanned for np scatterings that occurred within $\pm 3^\circ$ of the predicted direction

in all three views.*

The scanning was performed rapidly by using a special device designed and built for this experiment. An image of Figure 18 was projected onto the screen of the scanning projector in such a way that the apex of the "V" could be superimposed on the decay vertex by moving a single handle. The orientation of the "V" in the protractor was controlled by a large knob mounted on the scanning projector.

The scanners were requested to record only those events in which the projected length of the proton (on the scanning projector with a magnification of 2/3) was at least 2mm in one view and not less than 1mm in any view. Both scanning efficiency and measuring accuracy are poor for very short protons; we therefore increased the above lengths to 4mm and 2mm respectively for those events actually used in the determination of Φ.

The above selection procedure was very effective. From a total of 43 000 x 20 = 860 000 np scatterings only approximately 4300 events satisfying the scanning criteria were found. The recoil protons were measured and the results of these measurements were merged with the original measurements of Σ production and decay. The resulting data were subjected to a seven-constraint (7C) three-vertex fit. In some cases, which constitute 4% of the fitted events, the momentum of the

---

*In almost all cases the direction of the neutron can be predicted to better than 1°. In those cases in which it cannot, the $\pm 3^{\circ}$ scanning criterion was extended to ± 3 std. dev.

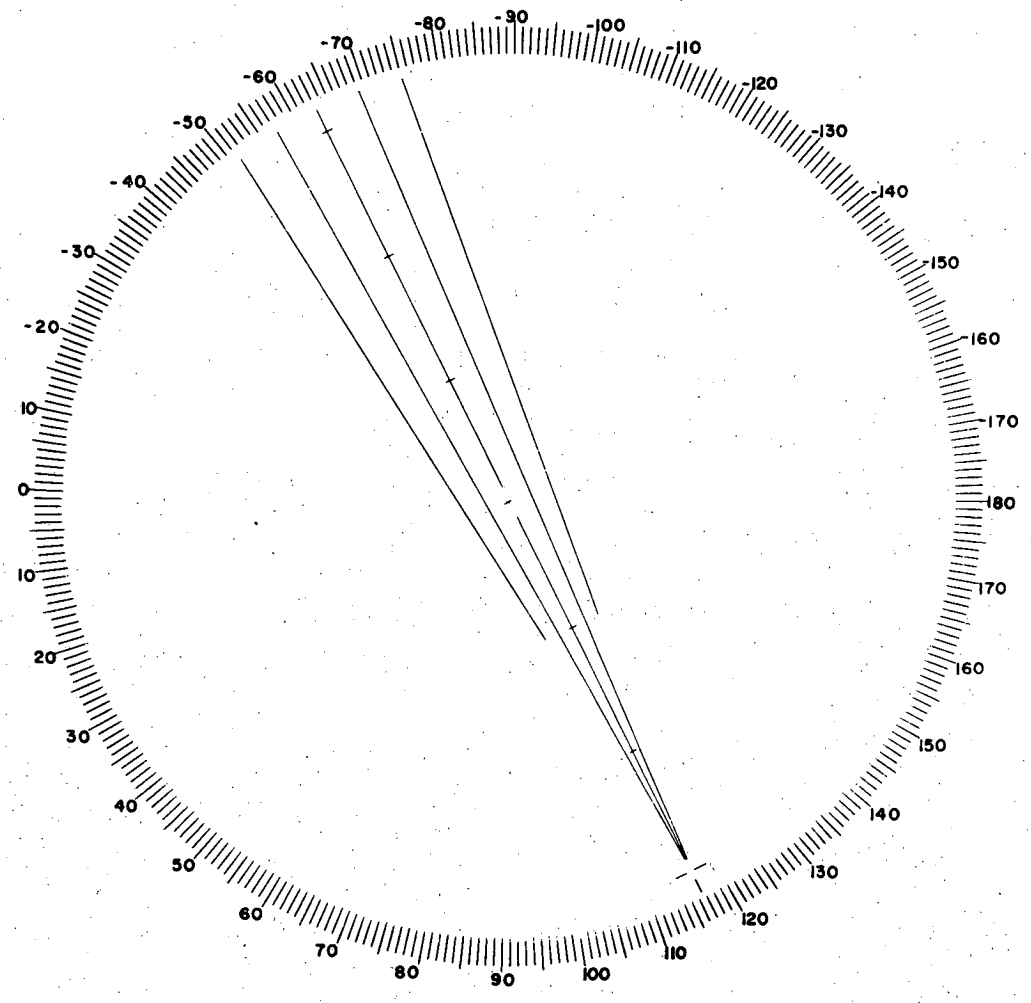

XBL 696-616

Fig. 18. Protractor used in scanning for np scatterings.

recoil proton cannot be measured with sufficient accuracy to provide any real constraint. These events were fitted using only 6 constraints. We obtain a final sample of 1385 Σ^- events and 560 Σ^+ events. The distributions of these events in kinetic energy and scattering angle are shown in Figure 19. The contours are curves of equal A.

B. Estimation of Background

The original fit to Σ production and decay is 4C,* and as noted, this fit determines both the direction and momentum of the neutron. Two of the three additional constraints imposed by measuring the np scattering can be regarded as coming from the measurement of the position of the np interaction point. Since the position of the $\Sigma \rightarrow n\pi$ vertex is known, this is equivalent to measuring the two angles specifying the direction of the neutron.

The neutron momentum and measurement of the np scattering angle determine the proton momentum. Measurement of this momentum provides the third additional constraint.

We estimate (see Appendix B) that the accuracy with which the direction of the neutron is known is alone sufficient to reduce background contamination to 10%. In order to investigate the elimination of background effected by all three constraints, we subtract χ^2 for the 4C fit (χ^2_4) from χ^2 for the final 7C (6C) fit. It can be shown

---

*The length of the Σ is typically too short to permit a useful momentum measurement; otherwise the fit to Σ production and decay would be 5C.

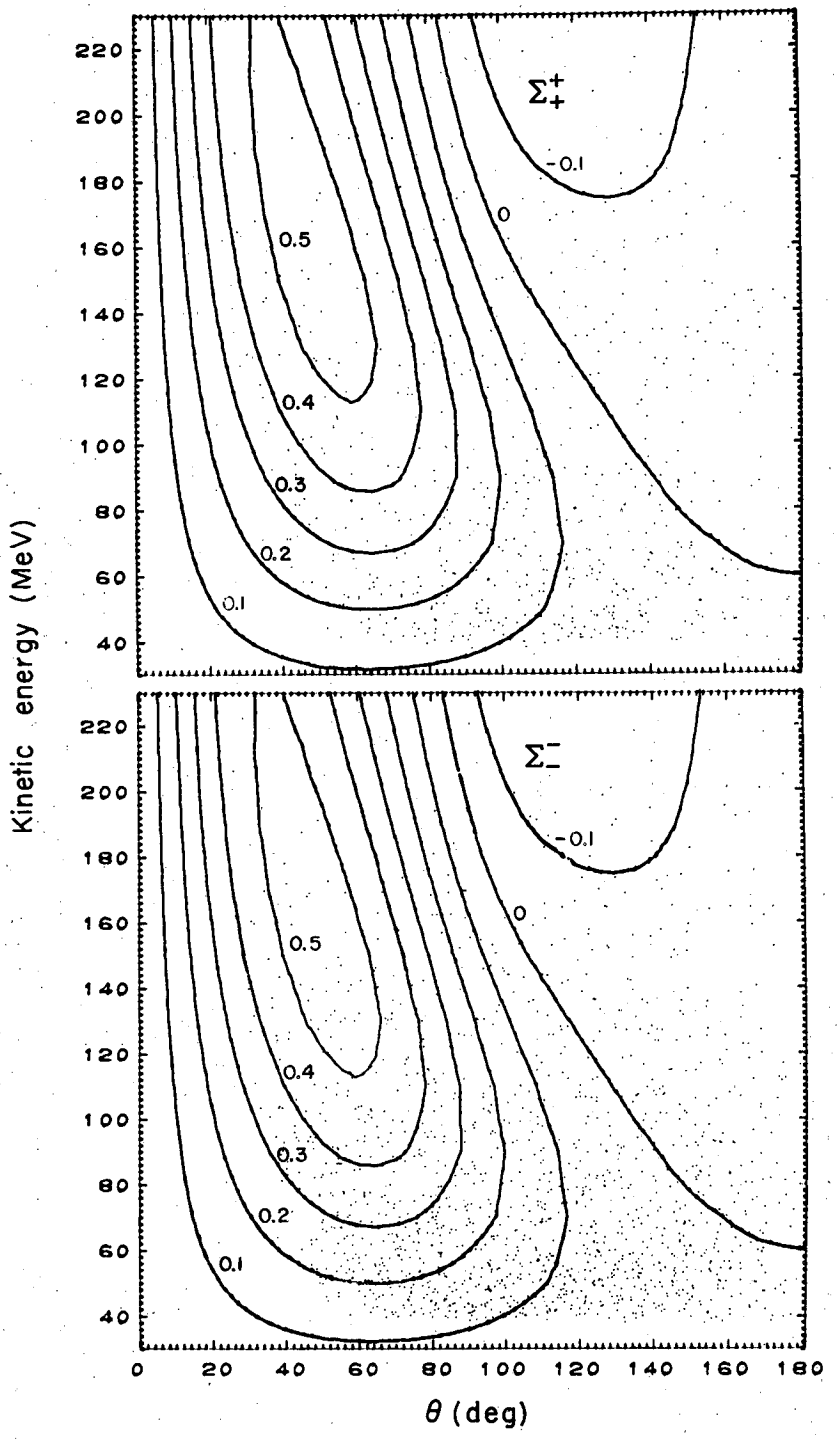

XBL 697-857

Fig. 19. Distributions of np scatterings in kinetic energy and scattering angle. The curves are contours of equal A.

(see Appendix C) that this difference is distributed as χ^2_3 (χ^2_2). The experimental χ^2 distributions together with the expected distributions are shown in Figure 20. The experimental distributions are too narrow indicating a slight overestimation of uncertainties. After examining these curves we decided to reject those events falling in the shaded areas of Figure 20.

The χ^2 distribution for n degrees of freedom is given by

$$W_n(\chi^2)d\chi^2 \propto e^{-\chi^2/2} (\chi^2)^{n/2-1} d\chi^2 \qquad (13)$$

If the background is random rather than Gaussian, the χ^2 distribution for background events by comparison with (13) is given by

$$W_n(\chi^2)d\chi^2 \propto (\chi^2)^{n/2-1} d\chi^2 \quad . \qquad (14)$$

The background is of course not truly random, but has some probability density function of finite width. An analysis of the distributions of the background events, including the effects of the $\pm 3^o$ scanning criterion, indicates that the deviations from (14) for $(\chi^2_7 - \chi^2_4) < 20$ or for $(\chi^2_6 - \chi^2_4) < 20$ are very small.

We obtain an upper limit on contamination of 2.9% by normalizing (14) to the shaded areas in Figure 20 assuming that all events in these areas are background. This should be a considerable overestimation for two reasons: The number of true events falling in this region is predicted by (13) to be about 2% of the total. Allowing for the overestimation of errors one expects this to be reduced to 1/2 - 1%. In addition the χ^2 distributions for bubble chamber experiments, in our experience, always have considerably more genuine events with large χ^2

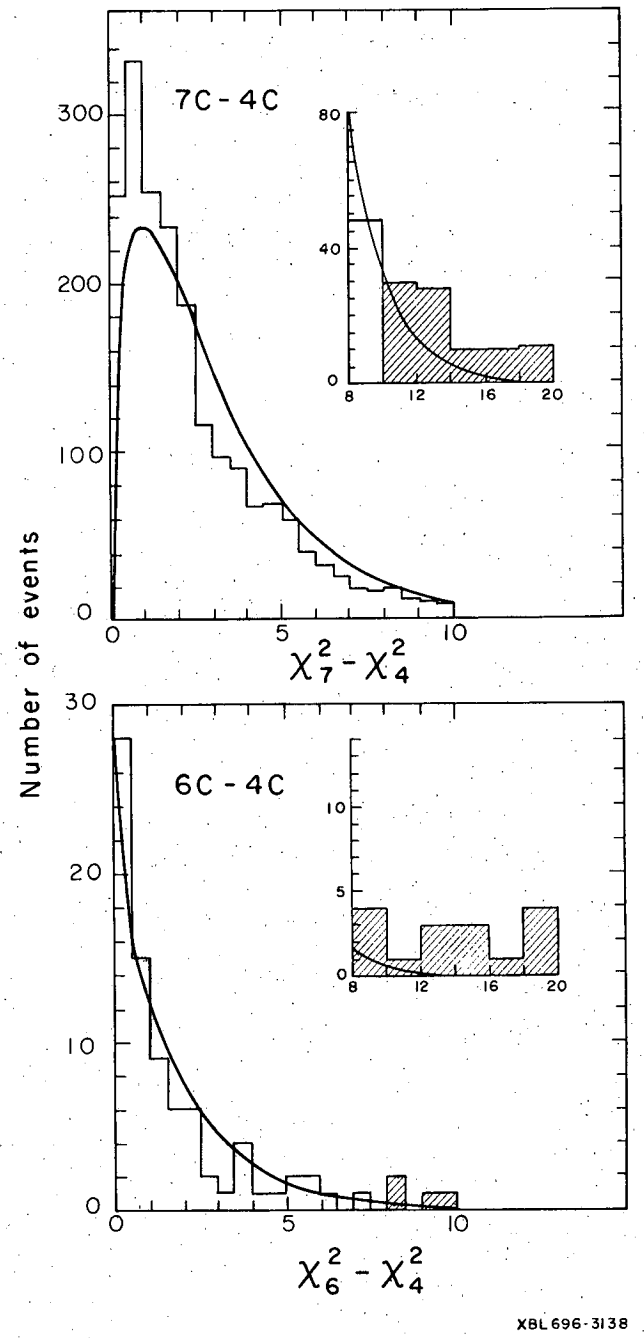

Fig. 20. Histograms of $\chi_7^2 - \chi_4^2$ and $\chi_6^2 - \chi_4^2$. The curves are the expected distributions. Events falling in the shaded areas are rejected.

than equation (13) predicts.

As final check on the effect of background the unshaded areas in Figure 20 were both extended to $\chi^2 = 16$. According to (14) this doubles the background in the sample, but results in a shift in Φ_+ and Φ_- of less than 8% of the statistical uncertainty. We conclude that the effects of background are truly negligible.

C. Investigation of Biases

In addition to contamination, the opposite problem of less of real events could also produce a bias.

One expects the three major sources of loss to be:

1. Bad measurements
2. Scanning inefficiency
3. Loss of protons that leave the bubble chamber close to the point of interaction.

The problem of bad measurements was considerably mitigated by carefully inspecting, and remeasuring, if necessary, all those events in which the recoil proton could not be successfully reconstructed from the original measurements. Altogether, 18% of the original 4300 events were remeasured.

Scanning efficiency and loss of particles that leave the bubble chamber shortly after scattering should both be primarily functions of the projected length of the recoil proton. In order to investigate these effects, 16% of our film was rescanned. Scanning efficiencies based on the two scans show a striking deficiency of short protons. However, since scanners on both scans tend to miss the same events and

because of insufficient data, efficiencies based on this method are not reliable.

Since np cross sections and polarizations are well known, we decided to obtain detection efficiencies by comparing the outcome of the actual experiment with the results of a Monte Carlo simulation.

The neutron from each of the 43 000 original Σ decays was propagated through the bubble chamber ten times producing about 33 000 fake np scatterings distributed according to the known cross section. The differential cross section depends on $\vec{P}_n$, which in turn is a function of Φ and P_Σ. The Monte Carlo simulation was performed for several extreme combinations of Φ and P_Σ. Fortunately all simulations give essentially the same detection efficiencies.

The detection efficiency e is given by

$$e = 10(\text{number of true events})/(\text{number of Monte Carlo events}).$$

Note that this is an overall detection efficiency and includes losses due to all effects. We find e to be a function of two parameters. The first, as expected, is the projected length. Since the scanners scanned in only one view unless an event was found, the projected length was taken to be the length in this view. Additionally, we find that those protons which dip steeply in the chamber are preferentially missed. This is presumably because the photographic perspective is such that these tracks appear considerably different in the three views and are not recognized as the same event by the scanners. The detection efficiency as a function of projected length for those protons with dip angles λ less than and greater than 45° is shown in Figure 21.

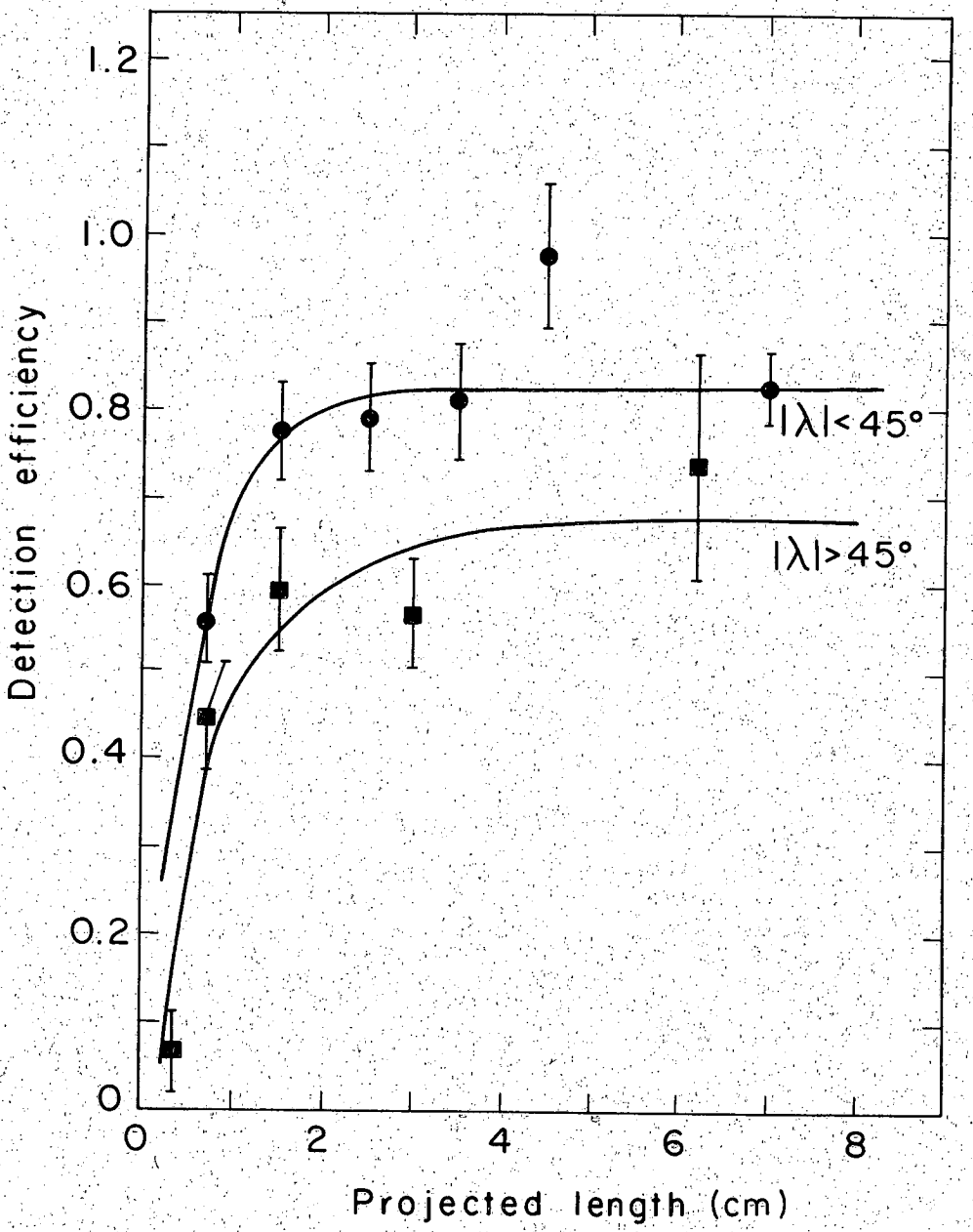

XBL696-3139

Fig. 21. Detection efficiency for recoil protons as a function of projected length and dip angle.

The curves are freehand and reflect the belief that the detection efficiency as a function of projected length should increase monotonically and then plateau.

D. Maximum Likelihood Determination of Φ

The probability density (12) must now be altered to include the effects of detection efficiency. We represent e as a function of ζ and a set of parameters y, describing all other relevant aspects of a particular event. Let Q(y) be the probability density for y. Then (12) becomes

$$W(\Phi, \zeta)d\zeta = \frac{\left[1 + AP_n(\Phi)\cos\zeta\right]\int e(\zeta,y)Q(y)dy}{\int\left[1 + AP_n(\Phi)\cos\zeta\right] e(\zeta,y)Q(y)d\zeta dy}\, d\zeta \,. \qquad (15)$$

We form the likelihood function $\mathcal{L}(\Phi)$ using equation (15). Neglecting terms independent of Φ, ln $\mathcal{L}(\Phi)$ is given by

$$\ln \mathcal{L}(\Phi) = \sum \ln\left[1+AP_n(\Phi)\cos\zeta\right] - N \ln \int \left[1+AP_n(\Phi)\cos\zeta\right] e(\zeta,y)Q(y)d\zeta dy$$

The sum extends over the total number of events N. This sum is just the usual expression for ln $\mathcal{L}(\Phi)$ while the second term contains all corrections.

Using (5) we rewrite the integral in the second term as

$$\int\left[1 + AP(\Phi)\cos\zeta\right] e(\zeta,y)Q(y)d\zeta\, dy$$

$$= \int\left[1 + A\,\frac{(\alpha + \vec{P}_\Sigma\cdot\hat{q})\,\hat{q}\cdot\hat{s}}{1 + \alpha\,\vec{P}_\Sigma\cdot\hat{q}}\right] e(\zeta,y)Q(y)d\zeta\, dy$$

$$+ \cos\Phi \int A\left[\frac{\vec{P}_\Sigma\cdot\hat{s} - (\vec{P}_\Sigma\cdot\hat{q})(\hat{q}\cdot\hat{s})}{1 + \alpha\vec{P}_\Sigma\cdot\hat{q}}\right](1-\alpha^2)^{\frac{1}{2}} e(\zeta,y)Q(y)d\zeta\, dy$$

$$+ \sin\Phi \int A\left[\frac{\vec{P}_\Sigma \times \hat{q}\cdot\hat{s}}{1 + \alpha\vec{P}_\Sigma\cdot\hat{q}}\right](1-\alpha^2)^{\frac{1}{2}} e(\zeta,y)Q(y)d\zeta\, dy$$

where the integrals on the right-hand side of the equation are now independent of Φ. Denoting these integrals by I_1, I_2 and I_3 the expression for $\ln \mathcal{L}(\Phi)$ becomes

$$\ln \mathcal{L}(\Phi) = \sum \ln \left[1 + AP_n(\Phi)\cos \zeta \right] - N \ln(I_1 + I_2 \cos \Phi + I_3 \sin \Phi). \tag{16}$$

Since an analytic expression for $Q(y)$ is unknown, I_1, I_2 and I_3 were calculated using the 33 000 Monte Carlo events described above. The integrands if I_1, I_2 and I_3 depend on A, α, P_Σ, q, ζ , e and Q. Of these A, α, P_Σ, q and ζ are specified by each Monte Carlo event. For each event a numerical integration over ζ was performed by varying ζ between 0 and 2π. For each value of ζ the projected length and the dip of the recoil proton were calculated and e was obtained from the curves of Figure 21. Since the Monte Carlo events are distributed as $Q(y)$, I_1, I_2 and I_3 are approximated by summing the numerical integrations over all events. These sums are normalized by dividing by the total number of Monte Carlo events.

The logarithms of the corrected likelihood functions as given by (16) are shown in Figure 22. From these likelihood functions we obtain

$$\Phi_- = 14^\circ \pm 19^\circ,$$
$$\Phi_+ = 143^\circ \pm 29^\circ.$$

These values are practically unchanged for any reasonable values of α_- and α_+.

In view of the uncertainty in the detection efficiency e, one may question the entire correction procedure. However, Φ is quite

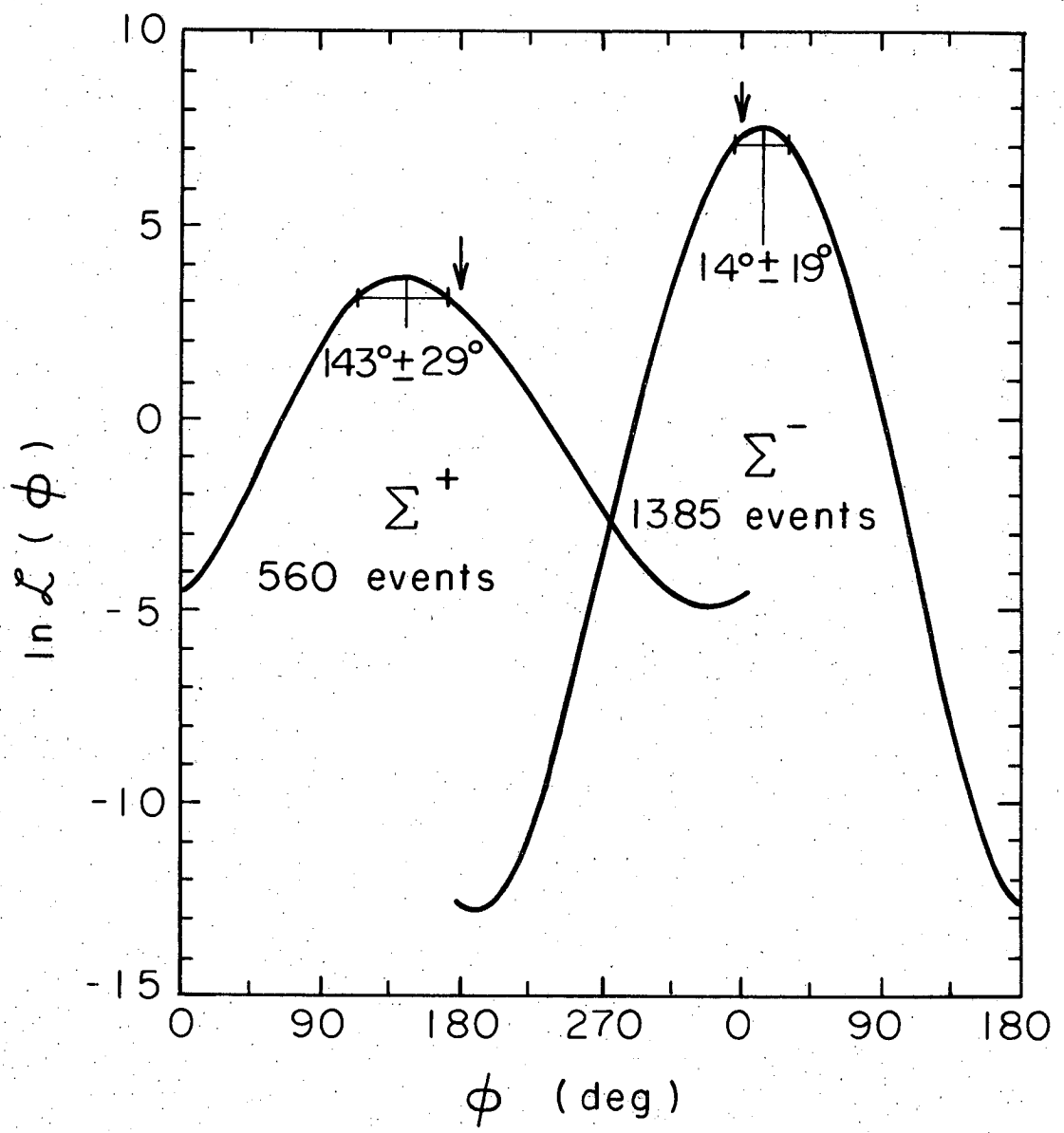

XBL696-3140

Fig. 22. Logarithm of likelihood functions used to determine Φ_- and Φ_+. The errors are determined by the points at which ln $\mathcal{L}(\Phi)$ decreases by 0.5.

insensitive to the corrections that have been applied. The uncorrected values are

$$\Phi_- = 15^\circ \pm 19^\circ,$$

$$\Phi_+ = 148^\circ \pm 28^\circ.$$

We were originally led to study the corrections because without them the following consistency check gave rather poor results.

Given Φ (the sign of γ) it is possible to regard (15) as a function of P_Σ, thus giving an additional check on the Σ^- polarization. As before, the sample is broken up into four bins according to predicted polarization. We obtain P_Σ for each bin, again using the maximum-likelihood method. The appropriate correction integrals for each bin were evaluated by using the same method as used in the measurement of Φ. Figure 23 exhibits the results with and without the corrections. Without the corrections the χ^2 confidence level is about 11%, while with corrections it is 67%. The corrections are only weakly dependent on the exact form of the detection efficiency functions. Despite the high confidence level for this consistency check we cannot rule out the possibility of some residual bias in our data; however, because of the insensitivity of Φ to the corrections that have been made any residual bias should be negligible.

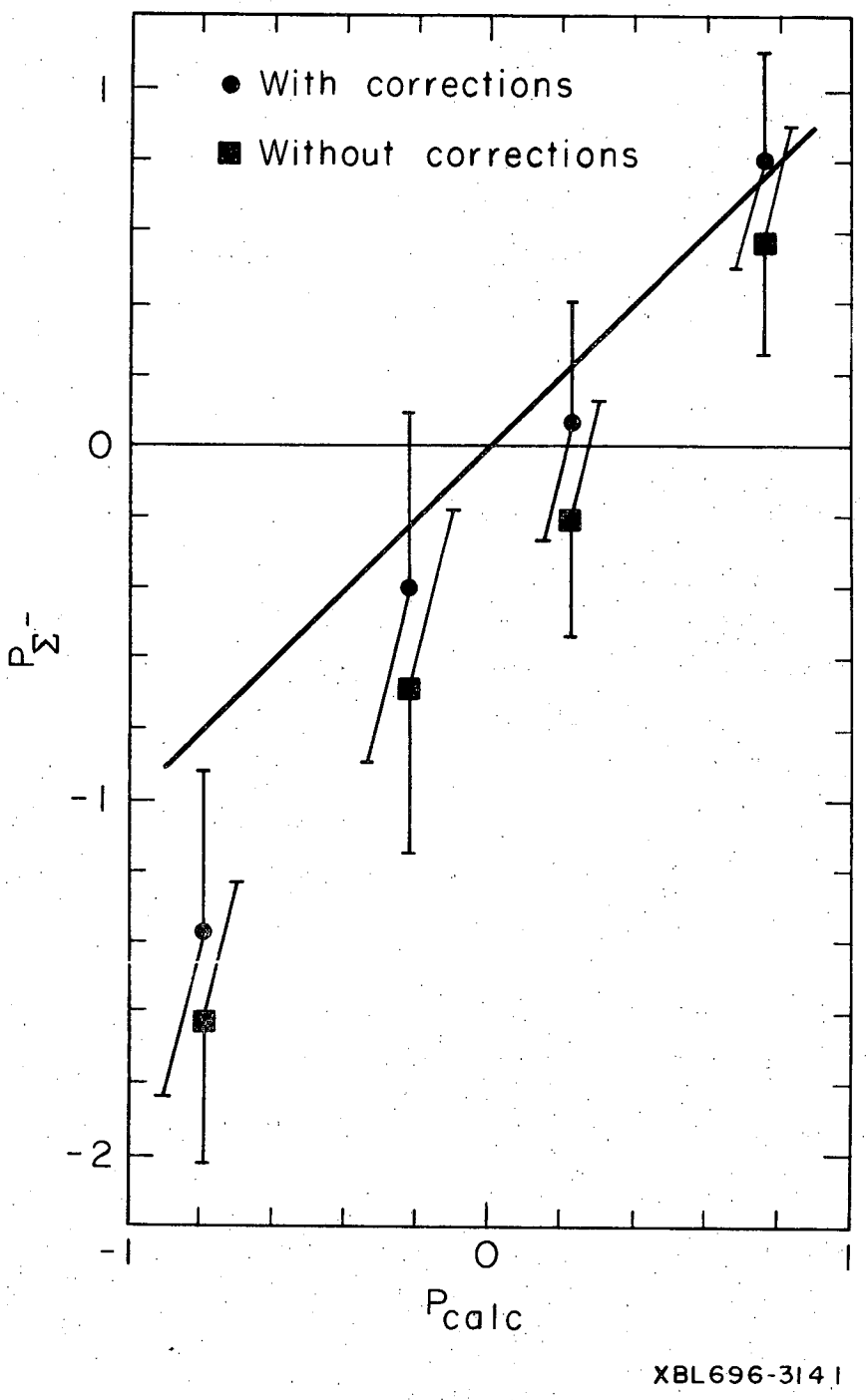

Fig. 23. Measured values of P_{Σ^-} as a function of the calculated value P_{calc}.

VI. THEORETICAL ANALYSIS AND CONCLUSIONS

Despite some formidable theoretical difficulties[12] it is generally assumed that the completely hadronic weak interactions can be described by a current-current type Hamiltonian density give by

$$H = J_\mu J_\mu^\dagger + J_\mu^\dagger J_\mu$$

where J_μ transforms like a member of an SU(3) octet. Since H is a symmetric form, it contains only the symmetric representations occurring in $8 \otimes 8$. These are 1, 8_s, and 27.

Although the three nonleptonic Σ decays all have $|\Delta I| = 1/2$, the isotopic spins can quite clearly be combined to give $|\Delta I| = 1/2$, 3/2 and 5/2. Both $|\Delta I| = 1/2$ and $|\Delta I| = 3/2$ can be accommodated in a Hamiltonian transforming as $8 \oplus 27$; however $|\Delta I| = 5/2$ cannot. Thus if one believes the octet current hypothesis, there is reason to expect $|\Delta I| = 5/2$ to be absent. The most economical way to explain the absence of $|\Delta I| = 3/2$ i.e., the $|\Delta I| = 1/2$ rule, is to assume that the entire 27 is absent (or at least that the 8 is strongly enhanced relative to the 27). There is no completely satisfactory explanation of why this should be so, and the extent to which it is true merits further investigation.

Assuming $|\Delta I| = 5/2$ is absent, we calculate the consequences of a Hamiltonian having both $|\Delta I| = 1/2$ and $|\Delta I| = 3/2$ contributions. Thus, since $\Delta I_z = -1/2$, the Hamiltonian has parts transforming as $|1/2,-1/2\rangle$ and $|3/2,-1/2\rangle$. The notation is $|I, I_z\rangle$.

Applying standard Condon and Shortley Clebsch-Gordan coefficients,

one obtains the following isotopic decompositions of the πN final states:

$$\langle \pi^- N| = \langle 3/2, -3/2|$$
$$\langle \pi^o p| = \sqrt{2/3}\ \langle 3/2, 1/2| - \sqrt{1/3}\ \langle 1/2, 1/2|$$
$$\langle \pi^+ n| = \sqrt{1/3}\ \langle 3/2, 1/2| + \sqrt{2/3}\ \langle 1/2, 1/2|$$

Using these decompositions and the Wigner-Eckart theorem[13] we write the three nonleptonic decay amplitudes as

$$A_- = A_{13} - \sqrt{2/5}\ A_{33} \tag{17a}$$

$$A_o = \sqrt{2}\ A_{13}/3 + 4\sqrt{5}\ A_{33}/15 - \sqrt{2}\ (A_{11} + A_{31}/2)/3 \tag{17b}$$

$$A_+ = A_{13}/3 + 2\sqrt{10}\ A_{33}/15 + 2\ (A_{11} + A_{31}/2)/3 \tag{17c}$$

A_{ij} denotes a reduced matrix element where $i = 2|\Delta I|$ and $j = 2I_{\pi N}$. Since A_{11} and A_{31} appear only in the combination $A_{11} + A_{31}/2$, it is impossible to distinguish the two experimentally. It is sometimes convenient to combine equations (17) to give

$$\sqrt{2}\ A_o + A_+ - A_- = 3\sqrt{2/5}\ A_{33} \ . \tag{18}$$

Equations (17) and (18) hold for both s and p amplitudes. Furthermore, as we later explain, s and p are expected to be nearly real. We can therefore, to a good approximation, write (18) as a real vector equation in a space where s is the abscissa and p is the ordinate

$$\sqrt{2}\ \vec{A}_o + \vec{A}_+ - \vec{A}_- = 3\sqrt{2/5}\ \vec{A}_{33} \ . \tag{19}$$

If only $|\Delta I| = 1/2$ terms are present, then

$$\sqrt{2}\ \vec{A}_o + \vec{A}_+ - \vec{A}_- = 0 \tag{20}$$

and, as is well known, the three nonleptonic decay amplitudes form a closed triangle in s-p space.

Several assumptions are necessary to compare the above expressions with experimental data. The first problem encountered involves the exact form of the decay matrix element. We have previously written this matrix element as $T = s + p\,\vec{\sigma}\cdot\hat{q}$. One could equally well write $T = s + p'\vec{\sigma}\cdot\vec{q}$ where $\vec{q}$ is no longer a unit vector. This is of no consequence when discussing the decay of a single charge state; however, when comparing various charge states to each other, it can make a considerable difference. For example, the reaction $\Sigma^+ \to n\pi^+$ has $|\vec{q}| = 185$ MeV/c while $\Sigma^- \to n\pi^-$ has $|\vec{q}| = 193$ MeV/c, resulting in about a 4% difference in p and p'.

It is of course possible, and generally desirable, to use a covariant formulation of hyperon decay, but again the choice of matrix element is not unique. For example, one can write either

$$T = \bar{U}_N (A - B\gamma_5) U_\Sigma \tag{21}$$

or

$$T = \bar{U}_N (A' - B'\gamma_5)\gamma_\lambda U_\Sigma k^\lambda \tag{22}$$

where k^λ is the 4-momentum of the pion. In writing all covariant equations, we will use the conventions of Bjorken and Drell.[14] We will also let M, m, and μ be the masses of Σ, N, and π respectively.

Again when discussing a single charge state, it is irrelevant if we choose (21) or (22), since by use of the Dirac equation (22) can be expressed as

$$T = \left[\bar{U}_N \quad A'(M-m) - B'(M+m)\gamma_5 \right] U_\Sigma \quad .$$

This is equivalent to (21) with $A = A'(M-m)$ and $B = B'(M+m)$. Similarly, all more complicated matrix elements can be shown to reduce to (21). This must be so since the decay is completely specified by two parameters. Furthermore, A and B (or A' and B') are simply proportional to s and p respectively.

If we define

$$C_1 = \frac{1}{8\pi} \frac{q}{\mu^+} \frac{(M+m)^2 - \mu^2}{M^2}$$

and

$$C_2 = \frac{(M-m)^2 - \mu^2}{(M+m)^2 - \mu^2} ,$$

then the decay rate times the branching ratio is given by

$$b\Gamma = C_1(|A|^2 + C_2|B|^2) \tag{23}$$

and the decay parameters are given by

$$\alpha = \frac{2\sqrt{C_2}\ \mathrm{Re}(A^*B)}{|A|^2 + C_2|B|^2} \tag{24a}$$

$$\beta = \frac{2\sqrt{C_2}\ \mathrm{Im}(A^*B)}{|A|^2 + C_2|B|^2} \tag{24b}$$

$$\gamma = \frac{|A|^2 - C_2\ |B|^2}{|A|^2 + C_2\ |B|^2} \tag{24c}$$

We have defined C_1 and C_2 and thus A and B to be consistent with a summary by J. Peter Berge[15] that has been widely quoted in the litera-

ture.

If one replaces C_1 and C_2 by $C_1' = C_1(M-m)^2$ and $C_2' = C_2 \left[(M+m)/(M-m)\right]^2$, equations (23) and (24) also hold for A' and B'.

Another problem complicating the comparison of different charge states comes from the nature of A and B. The quantities A and B (or A' and B') are really form factors and may depend on momentum transfer, which is different for different charge states. In absence of an adequate theory, we neglect this dependence.

Since the weak interaction is thought to be of the current-current form, (22) may seem more fundamental than (21). However, until we have a theory which specifies how to correct for the lack of exact symmetry among various charge states, there is really no reason to prefer (22) or some other interaction over (21). We will give results for both (21) and (22) and ignore the nonrelativistic parameters. All of our comments about isospin, particularly equations (17) through (20), are of course valid for A and B (or A' and B') as well as s and p.

In the derivation of equations (17) through (20) we referred only to symmetries of the weak Hamiltonian. Unfortunately, both strong and electromagnetic interactions influence the physically measured decay parameters.

The electromagnetic radiative corrections have been calculated by C. Jarlskog.[16] Although this calculation is dependent on an unknown cutoff parameter, it seems certain that the corrections to both A and B are considerably less than 1% for all three decay modes. We therefore neglect these effects.

If one writes the S-matrix as $S = 1+2iT$, unitarity implies that $-i(T-T^{\dagger}) = 2TT^{\dagger}$. If one assumes time reversal invariance, then $T_{ab} = T_{ba}$, thus $\mathrm{Im}(T_{ab}) = \sum_n T_{an}T_{nb}^{*}$. Let b be an initial Σ state and a be a specific isotopic spin state of the $N\pi$ system. If one evaluates the matrix elements at the Σ decay energy, the strong process $N\pi \rightarrow N\pi$ is overwhelmingly dominant and one may write

$$\mathrm{Im}(T_{ab}) = T_{ab}T_{bb}^{*} = T_{ab}|T_{bb}|\, e^{-i\delta} \qquad (25)$$

where δ is the appropriate $N\pi$ phase shift. Since $\mathrm{Im}(T_{ab})$ is real, the phase of T_{ab} is given by δ (modulo π). Also then the relative phase of A and B is given by $\Delta = \delta_p - \delta_s$ (again modulo π).

In principle, one can measure α and β and determine $\Delta = \tan^{-1}(\beta/\alpha)$, thus providing a test of time reversal invariance. Combining our measurements of α and Φ with those in Table I, we obtain $\Delta_- = -43\ ^{+\ 113}_{-\ 35}$ deg and $\Delta_+ = 80\ ^{+\ 5}_{-\ 102}$ deg. The uncertainties are too large to provide a test of time reversal invariance.

For our purposes, we assume equation (25) is exact. This assumption should be very good. The only processes in which a violation of CP (or T from the CPT theorem) invariance has been established are decays of neutral K mesons. In these decays the CP noninvariant amplitudes are of the order of 10^{-3} as large as the CP conserving amplitudes. Perhaps more relevant to Σ decay is the measurement of Δ for other hyperon decays. In particular Δ for Λ decay has been measured to be (-7.5 ± 3.9) degrees[3] in excellent agreement with equation (25).

We note in passing that all $N\pi$ phase shifts at Σ decay energies are small justifying our earlier comment about the nearly real nature of the decay amplitudes.

Subject to the uncertainties and reservations stated, we are now in a position to express the measured parameters in terms of theoretical amplitudes. There are eight statistically-independent measured quantities: α_-, α_o, α_+/α_o, Γ_-, $\Gamma_{total} = \Gamma_o + \Gamma_+$, $b = \Gamma_+/\Gamma_{total}$, Φ_-, and Φ_+. The parameter α_- is given by

$$\alpha_- = \frac{2\sqrt{C_2^-}\ \mathrm{Re}\ (A_{13} - \sqrt{2/5}\ A_{33})(B_{13} - \sqrt{2/5}\ B_{33})\, e^{i(\delta_{31} - \delta_3)}}{(A_{13} - \sqrt{2/5}\ A_{33})^2 + C_2^- (B_{13} - \sqrt{2/5}\ B_{33})^2}$$

$$= 2C_1^- \sqrt{C_2^-} \cos(\delta_{31} - \delta_3)(A_{13} - \sqrt{2/5}\ A_{33})(B_{13} - \sqrt{2/5}\ B_{33})/\Gamma_- . \qquad (26a)$$

The πN phase shifts are denoted by $\delta_{2I,L}$ and A_{ij} and B_{ij} now represent purely real quantities. Similarly, one may write

$$\alpha_o = 2C_1^o \sqrt{C_2^o} \Big[\cos(\delta_{13}-\delta_3)(\sqrt{2}\,A_{13}/3 + 4\sqrt{5}\,A_{33}/15)(\sqrt{2}B_{13}/3 + 4\sqrt{5}B_{33}/15)$$
$$- \cos(\delta_{11}-\delta_3)(\sqrt{2}\,A_{13}/3 + 4\sqrt{5}\,A_{33}/15)(\sqrt{2}/3)(B_{11}+B_{31}/2)$$
$$- \cos(\delta_{31}-\delta_1)(\sqrt{2}/3)(A_{11}+A_{31}/2)(\sqrt{2}\,B_{13}/3 + 4\sqrt{5}\,B_{33}/15)$$
$$+ \cos(\delta_{11}-\delta_1)(2/9)(A_{11}+A_{31}/2)(B_{11}+B_{31}/2) \Big] / \Gamma_o \ , \qquad (26b)$$

$$\alpha_+ = 2C_1^+ \sqrt{C_2^+} \Big[\cos(\delta_{13}-\delta_3)(A_{13}/3 + 2\sqrt{10}\,A_{33}/15)(B_{13}/3 + 2\sqrt{10}\,B_{33}/15)$$
$$+ \cos(\delta_{11}-\delta_3)(A_{13}/3 + 2\sqrt{10}\,A_{33}/15)(2/3)(B_{11}+B_{31}/2)$$
$$+ \cos(\delta_{31}-\delta_1)(2/3)(A_{11}+A_{31}/2)(B_{13}/3 + 2\sqrt{10}\,B_{33}/15)$$
$$+ \cos(\delta_{11}-\delta_1)(4/9)(A_{11} + A_{31}/2)(B_{11} + B_{31}/2) \Big] / \Gamma_+ \ , \qquad (26c)$$

$$\Gamma_- = C_1^- \left[(A_{13} - \sqrt{2/5}\, A_{33})^2 + C_2^- (B_{13} - \sqrt{2/5}\, B_{33})^2 \right], \qquad (26d)$$

$$\begin{aligned}\Gamma_o = {} & C_1^o \Big\{ \Big[(\sqrt{2}\, A_{13}/3 + 4\sqrt{5}\, A_{33}/15)^2 + (2/9)(A_{11} + A_{31}/2)^2 \\ & - 2\cos(\delta_3 - \delta_1)(\sqrt{2}\, A_{13}/3 + 4\sqrt{5}\, A_{33}/15)(\sqrt{2}/3)(A_{11} + A_{31}/2) \Big] \\ & + C_2^o \Big[(\sqrt{2}\, B_{13}/3 + 4\sqrt{5}\, B_{33}/15)^2 + (2/9)(B_{11} + B_{31}/2)^2 \\ & - 2\cos(\delta_{31} - \delta_{11})(\sqrt{2}\, B_{13}/3 + 4\sqrt{5} B_{33}/15)(\sqrt{2}/3)(B_{11} + B_{31}/2) \Big] \Big\}, \end{aligned} \qquad (26e)$$

$$\begin{aligned}\Gamma_+ = {} & C_1^+ \Big\{ \Big[(A_{13}/3 + 2\sqrt{10}\, A_{33}/15)^2 + (4/9)(A_{11} + A_{31}/2)^2 \\ & + 2\cos(\delta_3 - \delta_1)(A_{13}/3 + 2\sqrt{10}\, A_{33}/15)(2/3)(A_{11} + A_{31}/2) \Big] \\ & + C_2^o \Big[(B_{13}/3 + 2\sqrt{10}\, B_{33}/15)^2 + (4/9)(B_{11} + B_{31}/2)^2 \\ & + 2\cos(\delta_{31} - \delta_{11})(B_{13}/3 + 2\sqrt{10}\, B_{33}/15)(2/3)(B_{11} + B_{31}/2) \Big] \Big\}, \end{aligned} \qquad (26f)$$

$$\Phi_- = \tan^{-1}(\beta_- \Gamma_- / \Upsilon_-), \qquad (26g)$$

and

$$\Phi_+ = \tan^{-1}(\beta_+ \Gamma_+ / \Upsilon_+). \qquad (26h)$$

The expressions for β_- and β_+ are obtained by making the replacement cos → sin in (26a) and (26c). The expressions for Υ_- and Υ_+ are obtained by making the replacement $C_2 \rightarrow -C_2$ in (26d) and (26f).

If we assume the Nπ phase shifts are precisely known, equations (26) can be used to express the eight measured quantities in terms of six unknown amplitudes ($A_{11} + A_{31}/2$ is regarded as a single parameter).

We will perform a χ^2 minimization to obtain the best fitted values of the amplitudes.

Table III is a compilation of the data in Table I, together with our new data.

Table III

Reaction	α	Φ	Γ_{total}	b
$\Sigma^- \to n\pi^-$	$-.074 \pm .011$	$(4 \pm 16)^\circ$	$(.604 \pm .011) \times 10^{10}$/sec	1.00
$\Sigma^+ \to p\pi^o$	$-.995 \pm .022$		$(1.235 \pm .020) \times 10^{10}$/sec	$0.528 \pm .015$
$\Sigma^+ \to n\pi^+$	$\alpha_+/\alpha_o = -.059 \pm .015$	$(161 \pm 21)^\circ$	$(1.235 \pm .020) \times 10^{10}$/sec	$0.472 \pm .015$

The πN phase shifts are given by[17]

$$\delta_1 = 9^\circ \qquad \delta_{11} = 0^\circ \qquad \delta_3 = -12^\circ \qquad \delta_{31} = -3^\circ$$

The familiar AB trangle representation of the data is shown in Figure 24.

Equations (26g) and (26h) and the measurements of $\Phi_\pm$ are extremely important in eliminating the so-called "which is which" ambiguity. It has been known for many years that $\alpha_- \approx \alpha_+ \approx 0$. Thus these decays are nearly pure s-wave or pure p-wave. Assuming the $|\Delta I| = 1/2$ rule (equation (20)), the known α parameters and decay rates demand that if $\Sigma^- \to n\pi^-$ is mostly s-wave, $\Sigma^+ \to n\pi^+$ must be mostly p-wave and vice versa. Without a measurement of Φ_+ or Φ_- there is no direct way[18] of determining which is which.

In two very influential papers[2] Sugawara and Suzuki used the

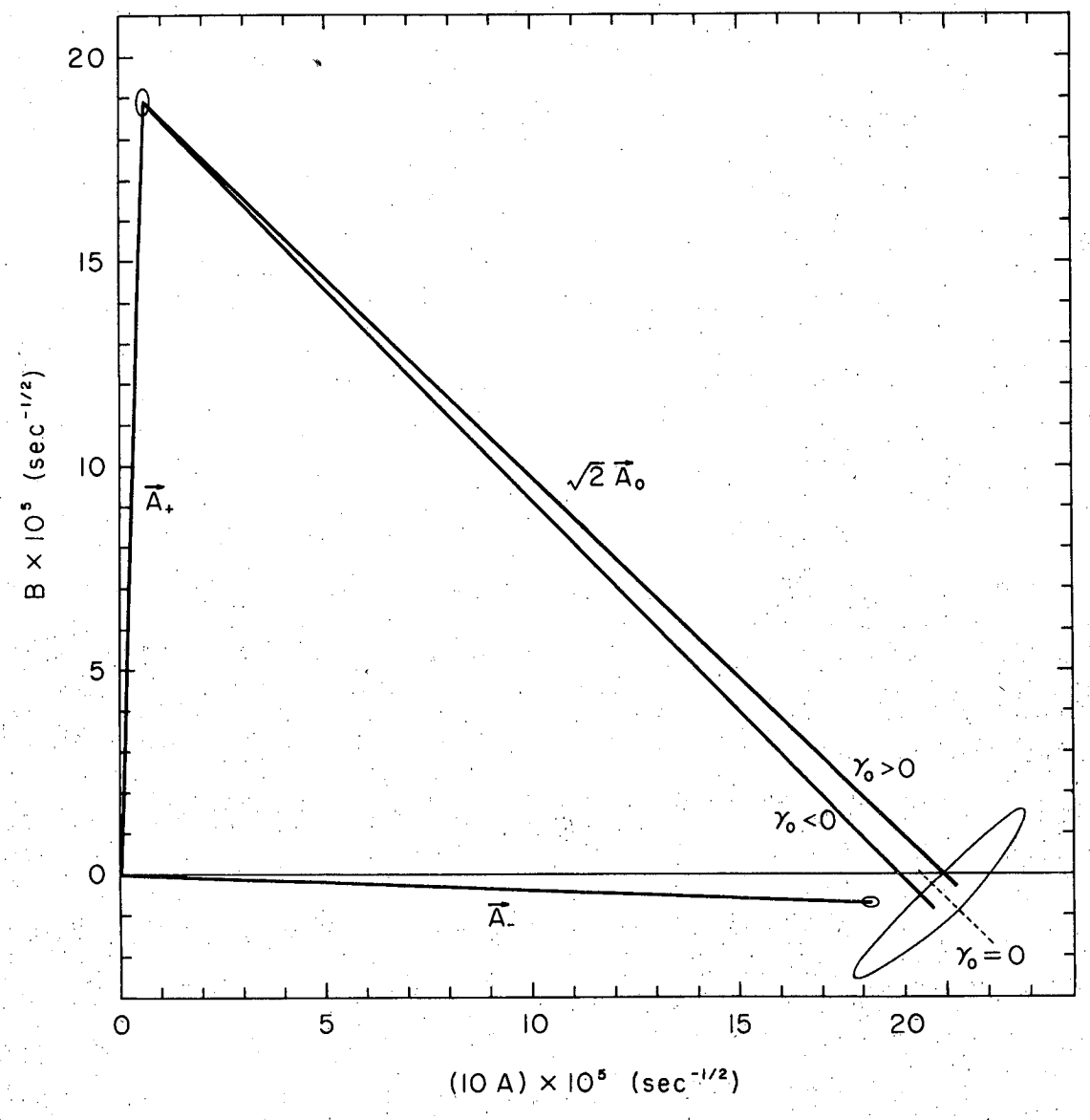

XBL 697-866

Fig. 24. The $\Delta I = 1/2$ triangle in A-B space. Only the real parts of the amplitudes are shown. The elipses indicate the uncertainty in the amplitudes.

algebra of currents to theoretically predict that $A_+ = 0$. The measurements of Φ_+ have provided striking confirmation of this prediction, but unfortunately the experimental uncertainties in $\Phi_\pm$ are still so large that these measurements contribute practically nothing to the precision with which one can determine the A and B amplitudes.

Since γ_o has not been measured, there could still be one remaining ambiguity in the solution of equations (26) corresponding to $\gamma_o > 0$ and $\gamma_o < 0$. We find $\alpha_o \approx -1$ so that $\gamma_o \approx 0$ and the two solutions are essentially the same.

Using the data in Table III, we have performed six different fits to equations (26). The results are tabulated in Table IV.

In fits 1 and 2, we have set $A_{33} = B_{33} = 0$ and assumed the sign of γ_o which resulted in the lowest χ^2. If one also assumes that $A_{31} = B_{31} = 0$, these two fits are tests of the $|\Delta I| = 1/2$ rule and indicate that to the accuracy of the present data there is no need to invoke $|\Delta I| = 3/2$.

Since A and B are very insensitive to our measured values of $\Phi_\pm$, fits 3 through 6 involve no real constraints and are to be regarded simply as solutions of equations (26). These solutions indicate clearly the extent to which the $|\Delta I| = 3/2$ amplitudes are known.

In addition to the above fits we have performed a fit similar to fit 3 but neglecting the measurements of $\Phi_\pm$. From this fit we find the expected values of $\Phi_\pm$ to be given by $\Phi_- = -0.7^\circ$ and $\Phi_+ = 165.7^\circ$. These values are to be contrasted with the expected values $\Phi_- = 0^\circ$ and $\Phi_+ = 180^\circ$ obtained by neglecting final state interactions. Note that $\beta_+ > \alpha_+$. This condition results from the fact that the real parts

Table IV. Fitted values of Σ decay amplitudes. Matrix element SP refers to the scalar-pseudoscalar interaction (21) and VA refers to the vector-axialvector interaction (22). Amplitudes A and B for the SP interaction are given in units of 10^5 $sec^{-1/2}$ and amplitudes A' and B' for the VA interaction are given in units of 10^5 GeV^{-1} $sec^{-1/2}$.

Fit	Matrix Element	$A_{11} + A_{31}/2$	$B_{11} + B_{31}/2$	A_{13}	B_{13}	A_{33}	B_{33}	Degrees of Freedom	χ^2	γ_o
1	SP	-0.844 ±0.023	29.46 ±0.32	1.865 ±0.017	-0.710 ±0.102	0	0	4	3.44	<0
2	VA	-3.275 ±0.090	13.93 ±0.15	7.240 ±0.064	-0.334 ±0.048	0	0	4	5.58	< 0
3	SP	-0.905 ±0.069	28.90 ±0.72	1.905 ±0.047	-0.803 ±0.426	0.072 ±0.073	-0.185 ±0.670	2	0.13	< 0
4	VA	-3.613 ±0.254	13.56 ±0.32	7.467 ±0.174	-0.369 ±0.183	0.401 ±0.268	-0.076 ±0.288	2	0.13	< 0
5	SP	-0.953 ±0.040	28.40 ±0.48	1.937 ±0.028	-0.486 ±0.240	0.124 ±0.041	0.317 ±0.375	2	0.12	> 0
6	VA	-3.746 ±0.150	13.40 ±0.21	7.556 ±0.106	-0.268 ±0.102	0.542 ±0.155	0.084 ±0.159	2	0.12	> 0

Best Fitted Values of Measured Parameters for Fits 1 and 2.

Fit	α_-	α_o	α_+/α_o	Γ_-	Γ_{total}	b	Φ_-	Φ_+
1	-0.076	-0.988	-0.055	$.608 \times 10^{10}$	1.229×10^{10}	0.497	-0.69^o	166.89^o
2	-0.077	-0.984	-0.054	$.609 \times 10^{10}$	1.228×10^{10}	0.504	-0.70^o	167.37^o

of the two isotopic-spin amplitudes that make up A_+ nearly cancel each other.

All fits were performed using the program MINFUN,[19] which provides an estimate of the error matrix for the fitted parameters. The fitted parameters are rather strongly correlated, and we give the error matrices in Table V.

In conclusion, we note that since $\alpha_o \approx -1$, a small uncertainty in α_o results in a very large uncertainty in the angular orientation of the $\Sigma^+ \to p\pi^o$ amplitude in the AB plane. On the other hand, an accurate measurement of γ_o would precisely and uniquely determine the orientation of this amplitude. It is evident from the AB triangle that such a measurement would greatly improve our knowledge of the $|\Delta I| = 3/2$ amplitudes.

Table V. Error matrices for Σ decay amplitudes. The rows and columns are ordered as $A_{11} + A_{31}/2$, $B_{11} + B_{31}/2$, A_{13}, B_{13}, A_{33}, B_{33}.

ERROR MATRIX FOR FIT 1

.000516	.001947	-.000127	-.000009
.001947	.103807	-.001153	-.000110
-.000127	-.001153	.000275	-.000034
-.000009	-.000110	-.000034	.010370

ERROR MATRIX FOR FIT 2

.008169	.003450	-.001890	-.000011
.003450	.022480	-.001969	-.000009
-.001890	-.001969	.004131	-.000069
-.000011	-.000009	-.000069	.002274

ERROR MATRIX FOR FIT 3

.004780	.044101	-.003030	-.022127	-.004778	-.035136
.044101	.520674	-.029775	-.219495	-.046951	-.348532
-.003030	-.029775	.002248	.015129	.003244	.024091
-.022127	-.219495	.015129	.181389	.023909	.276857
-.004778	-.046951	.003244	.023909	.005354	.037911
-.035136	-.348532	.024091	.276857	.037911	.448495

Table V. Continued.

ERROR MATRIX FOR FIT 4

.064297	.069453	-.040214	-.032952	-.063380	-.052386
.069453	.100198	-.046857	-.038888	-.073844	-.061822
-.040214	-.046857	.030246	.022575	.043142	.036011
-.032952	-.038888	.022575	.033503	.035666	.050809
-.063380	-.073844	.043142	.035666	.071589	.056604
-.052386	-.061822	.036011	.050809	.056604	.082728

ERROR MATRIX FOR FIT 5

.001624	.013699	-.000883	-.003648	-.001383	-.005871
.013699	.231052	-.009139	-.041170	-.014304	-.066259
-.000883	-.009139	.000791	.002546	.000942	.004159
-.003648	-.041170	.002546	.057696	.004010	.081342
-.001383	-.014304	.000942	.004010	.001714	.006408
-.005871	-.066259	.004159	.081342	.006408	.140506

ERROR MATRIX FOR FIT 6

.022628	.021351	-.011954	-.004682	-.018698	-.007571
.021351	.045245	-.014384	-.006240	-.022468	-.010089
-.011954	-.014384	.011172	.003371	.013007	.005556
-.004682	-.006240	.003371	.010480	.005294	.014393
-.018698	-.022468	.013007	.005294	.023928	.008483
-.007571	-.010089	.005556	.014393	.008483	.025439

ACKNOWLEDGMENTS

I am very grateful to my advisor Prof. Robert D. Tripp for his constant help and guidance. I am also very grateful to Prof. M. Lynn Stevenson for serving as my advisor during the early stages of the experiment and for his continuing encouragement.

I appreciate the help of Dr. Angela Barbaro-Galtieri, Dr. Joseph J. Murray, and Dr. Frank T. Solmitz; and acknowledge the leadership and support of Prof. Luis W. Alvarez.

All of the above people have contributed greatly to my understanding and appreciation of physics, but I thank them most for the personal examples they have been to me and for their friendship.

I am indebted to the National Science Foundation and the Atomic Energy Commission for financial support.

I thank my fellow graduate students for many helpful and enjoyable discussions.

I am grateful to my parents, Mr. and Mrs. Myron O. Bangerter, for their constant encouragement and for first teaching me about "how and why."

Finally, I thank my wife and children, Sharon, Jamie, and Boyd, for their love and support.

This work was done under the auspices of the U. S. Atomic Energy Commission.

APPENDICES

A. Resolution of the $\Sigma_o^+ - \Sigma_+^+$ Ambiguity

The logarithm of the probability ratio r = (probability of Σ_+^+) / (probability of Σ_o^+) is given by

$$\log(r) = \sum_{i=1}^{7} \log\rho_i$$

The ratios ρ_i are determined by the 7 types of mass dependent information described in Section IV-B.

The quantity $\log\rho_1$ is determined by kinematical fitting and is given by

$$\log\rho_1 = .217\left[\chi^2(m_p)-\chi^2(m_\pi)\right] + \log\left[\frac{\sigma_\phi(m_p)\sigma_\lambda(m_p)\sigma_k(m_p)}{\sigma_\phi(m_\pi)\sigma_\lambda(m_\pi)\sigma_k(m_\pi)}\right] .$$

Note that $.217 = \frac{1}{2}\log(e)$. The full error matrix E is not available in TVGP output so that $\left[\det E(m_p)/\det E(m_\pi)\right]^{\frac{1}{2}}$ has been approximated using only the diagonal elements of E. These diagonal elements are given by σ^2. The subscripts ϕ, λ and k refer to the azimuth, dip and momentum of the charged decay particle.

The value of $\log\rho_2$ is determined by

$$\log\rho_2 = \begin{cases} -1.1, & |\lambda| \le 50^\circ \text{ and scanned as } \Sigma_o^+ \\ -.4, & |\lambda| > 50^\circ \text{ and scanned as } \Sigma_o^+ \\ .4, & |\lambda| \le 50^\circ \text{ and scanned as } \Sigma_+^+ \\ 1.1, & |\lambda| > 50^\circ \text{ and scanned as } \Sigma_+^+ \end{cases} .$$

Note that these values of $\log\rho_2$ somewhat underestimate the reliability of our scanners as given in Section IV.

The determination of $\log\rho_3$ is to some extent arbitrary and reflects our belief that less than .1% of those tracks that stop in the bubble chamber and give satisfactory fits to the Σ_o^+ hypothesis are in fact Σ_+^+ events. We have set

$$\log\rho_3 = \begin{cases} -3 \text{ for a stopping decay track} \\ 0 \text{ for a nonstopping decay track.} \end{cases}$$

The exact value of $\log\rho_3$ is relatively unimportant for our purposes. We require only that $|\log\rho_3|$ be large enough to effectively place events with stopping protons in the unambiguous category.

We define a χ^2 such that

$$\chi^2 = (p_f - p_\ell)^2/(\delta p_f)^2$$

where p_f is the fitted momentum of the proton from the Σ_o^+ hypothesis and δp_f is the associated uncertainty. The quantity p_ℓ is the momentum corresponding to a proton range equal to the measured length of the visible decay product. Since no corresponding χ^2 is available for the pion hypothesis we approximate it by its average value of 1 so that

$$\log\rho_4 = \begin{cases} .217(\chi^2 - 1), \; p_f < p_\ell \text{ and } \chi^2 > 1 \\ 0 \quad \text{otherwise.} \end{cases}$$

If $p_f > p_\ell$, χ^2 has no meaning since the visible decay track may be short simply because the particle leaves the bubble chamber. The condition $\chi^2 > 1$ insures that $\log\rho_4 > 0$. This is proper since the function of $\log\rho_4$ is to discriminate against those fits to the Σ_o^+ hypothesis that are not self-consistent.

Rather than attempt to interpret the track χ^2 described in

Section IV in a theoretical way, we have formed the quantity $\Delta = \chi^2(m_p) - \chi^2(m_\pi)$ and compared its distribution for tracks known to be protons with its distribution for tracks known to be pions. From these distributions we obtain

$$\log\rho_5 = \begin{cases} -0.3, & \Delta < -50 \\ 0, & -50 \leq \Delta \leq 10 \\ 1, & 10 < \Delta \leq 20 \\ 1.5, & 20 < \Delta \leq 40 \\ 2, & 40 < \Delta \end{cases}.$$

The distribution of Δ for ambiguous tracks could be somewhat different than the distribution for unambiguous tracks. To allow for this possibility we have made $|\log\rho_5|$ consistently smaller than the values obtained directly from the distributions.

The values of χ^2 obtained from the Spiral Reader measurements of bubble density are known to be rather unreliable, and we have consequently weighted this information very lightly. We define $x = .109 \left[\chi^2(m_p) - \chi^2(m_\pi) \right]$ and set

$$\log\rho_6 = \begin{cases} -1, & x < -1 \\ x, & -1 \leq x \leq 1 \\ 1, & 1 < x \end{cases}.$$

The value of $|\log\rho_6|$ has been limited to 1 since Spiral Reader information is less reliable than scanning information. For example if a track is crossed by other tracks in the bubble chamber, the Spiral Reader bubble density will be anomalously high.

Finally if $I_p(\hat{\Sigma} \cdot \hat{v})$ and $I_\pi(\hat{\Sigma} \cdot \hat{v})$ are respectively the laboratory distributions of $\hat{\Sigma} \cdot \hat{v}$ for Σ_o^+ and Σ_+^+ decays, $\log\rho_7$ is given by

$$\log\rho_7 = \begin{cases} \log(I_\pi/I_p), & -1 \leq \log(I_\pi/I_p) \\ -1, & \log(I_\pi/I_p) < -1. \end{cases}$$

We have demanded that $\log\rho_7 \geq -1$ to eliminate the well known "Jacobian peak" singularity.

If we also assign a value of $\log(r)$ to the kinematically unambiguous events we can directly calculate the ambiguity contamination in our samples. For unambiguous events we let $\log(r) = \log\rho_o + \log\rho_2$ where $\log\rho_2$ is defined above and

$$\log\rho_o = \begin{cases} -3 \text{ if kinematically unambiguous } \Sigma_o^+ \\ 3 \text{ if kinematically unambiguous } \Sigma_+^+. \end{cases}$$

For our experiment we have adjusted the various constants in SQUAW so that those mass hypotheses that are rejected are nearly always more than a factor of 10^3 less probable than the hypotheses that we accept. However, as in the case of $\log\rho_3$ the exact value of $\log\rho_o$ is relatively unimportant.

To the extent to which r is believable the fractional contamination of the Σ_o^+ sample of events is given by

$$C_o = \frac{1}{N_o} \sum_{i=1}^{N_o} \frac{1}{1 + \frac{1}{r_i}}$$

where N_o is the number of events having $r < 1$. Similarly the

contamination of the Σ_+^+ events is given by

$$C_+ = \frac{1}{N_+} \sum_{i=1}^{N_+} \frac{1}{1 + \frac{1}{r_i}}$$

where N_+ is the number of events having $r > 1$. We find

$$C_o = .00395$$

$$C_+ = .00347 .$$

Since we believe that we have systematically underestimated $|\log(r)|$ these should represent upper bounds on contamination. These bounds are consistent with the ambiguity scan described in Section IV.

B. Monte Carlo Simulation of np Scattering Background

Using Monte Carlo techniques, we have performed a calculation to determine the extent to which background is eliminated by the two constraints coming from the measurement of the position of the np scattering vertex.

The scanning projector was used to crudely measure the coordinates of about 150 background scatterings. As expected, we found these scatterings to be quite uniformly distributed in the bubble chamber.

For each of the 43 000 events originally scanned for recoils, we generated 10 fake randomly-distributed np scattering vertices. We calculated χ^2_2 for each vertex using the fitted neutron angles and uncertainties. For this calculation the position of each fake vertex was assigned an uncertainty corresponding to typical measurement uncertainties. This uncertainty is about .015 cm in x and y and about .05 cm in z.

Figure 25 is the χ^2 distribution for all fake events. The shaded area corresponds to those events satisfying the scanning criteria. Except for the effect of the scanning criteria the distribution is flat as predicted by equation (14). Also as asserted in Section V-B, significant deviations from (14) occur only for $\chi^2 > 20$. This is essentially because the width of the distribution of points selected by the scanning criteria is much wider than the uncertainty in neutron direction. The distributions of all the parameters (momentum and angles) of the background protons are much wider than the measured uncertainties in these parameters. One therefore expects (14) to be valid for

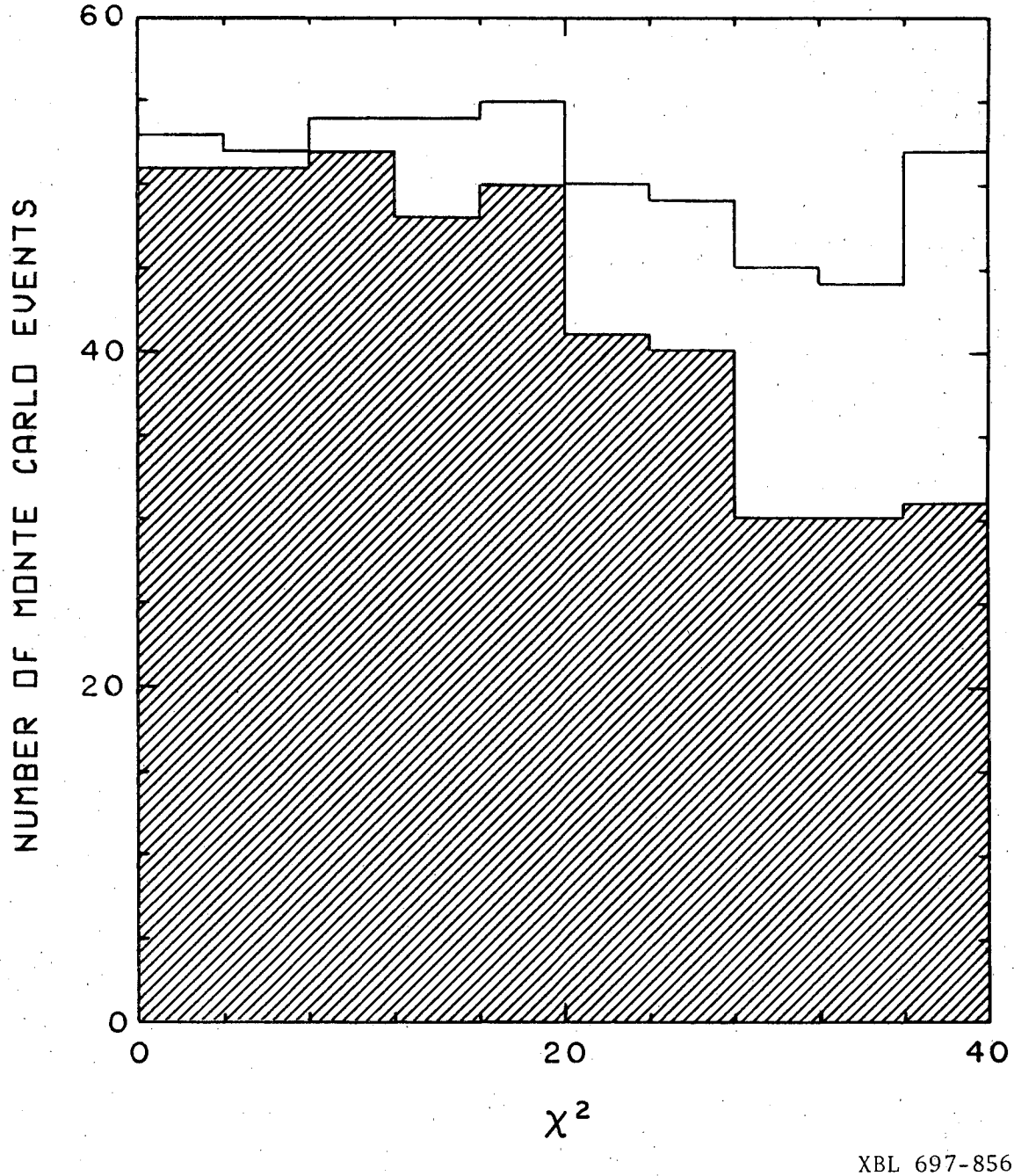

XBL 697-856

Fig. 25. Distribution of χ^2 for Monte Carlo up scatterings.

$(\chi_7^2 - \chi_4^2) < 20$ as well as $(\chi_6^2 - \chi_4^2) < 20$.

In the shaded area of Figure 25 there are 120 events having $\chi^2 < 10$. The Monte Carlo calculation explained in Section V-C shows that we should expect 3300 real events. Since there are about 20 rather than 10 recoils per frame the background should be 240/3300 = 7.3%. We emphasize again that this calculation neglects the additional powerful constraint imposed by momentum and energy conservation at the np vertex.

C. A Theorem on the Distribution of $\chi^2_m - \chi^2_n$

In working with multivertex fits to bubble chamber events it may sometimes be desirable to determine the effects of one particular vertex (or other subset of data) on the total goodness of fit. For example one may be certain of the interpretation given to some vertices but may be troubled with ambiguities or background at other vertices. The purpose of this appendix is to show that if one first applies an n-constraint fit to some subset of the data and then an m-constraint fit to the entire set of data, then $\chi^2_m - \chi^2_n$ is distributed as χ^2_{m-n}.

Before formally stating and proving this theorem, we briefly review the general χ^2 minimization problem.

Let ζ be the set of n measured parameters, and let α be the set of r parameters to be determined by minimizing χ^2. Also let E be the error matrix for ζ. As usual we assume that there is some linear transformation represented by a matrix f such that $\langle\zeta\rangle = f\alpha$. Then we have

$$\chi^2 = (\zeta - f\alpha)^\dagger E^{-1}(\zeta - f\alpha).$$

The matrix E (and thus E^{-1}) is symmetric and can therefore be diagonalized with an orthogonal matrix R. We rewrite χ^2 as follows:

$$\begin{aligned}\chi^2 &= (\zeta - f\alpha)^\dagger R^\dagger R E^{-1} R^\dagger R (\zeta - f\alpha) \\ &= (\zeta' - f'\alpha)^\dagger (E')^{-1}(\zeta' - f'\alpha)\end{aligned}$$

Since E' (and thus E'^{-1}) is positive definite one can define a matrix N such that $N^2 = (E')^{-1}$. The expression for χ^2 then becomes

$$\chi^2 = (\zeta' - f'\alpha)^\dagger NN(\zeta' - f'\alpha)$$

$$= (\xi - g\alpha)^\dagger(\xi - g\alpha)$$

$$= \eta^\dagger\eta$$

where $\xi = N\zeta'$, $g = Nf'$, and $\eta = \xi - g\alpha$. We have thus reduced χ^2 to a simple sum of squares.

Let α^* be the values of α which minimize χ^2. By differentiating χ^2 with respect to α one obtains

$$g^\dagger(\xi - g\alpha^*) = 0 .$$

If we define $G = g^\dagger g$ then $\alpha^* = G^{-1}g^\dagger\xi$ and χ^2 at its minimum value is given by

$$\chi_o^2 = \xi^\dagger(1 - gG^{-1}g^\dagger)^\dagger(1 - gG^{-1}g^\dagger)\xi$$

$$= \eta^\dagger(1 - gG^{-1}g^\dagger)^\dagger(1 - gG^{-1}g^\dagger)\eta$$

$$= \eta^\dagger P^\dagger P\eta$$

where $P = (1 - gG^{-1}g^\dagger)$. Note that $P = P^\dagger$ and also that

$$P^2 = (1 - gG^{-1}g^\dagger)(1 - gG^{-1}g^\dagger)$$

$$= 1 - 2gG^{-1}g^\dagger + gG^{-1}g^\dagger gG^{-1}g^\dagger$$

$$= 1 - gG^{-1}g^\dagger = P$$

so that P is a projection operator. Since P is symmetric it can be diagonalized by an orthogonal transformation. Furthermore since it is a projection operator all the eigenvalues are either 0 or 1 and $\chi_o^2 = \eta^\dagger P\eta$ can be represented as a sum of squares. It is well known[20] that χ_o^2 is a quadratic form in n-r dimensions. Thus the rank of P is n-r.

Theorem: Let ξ_1 and α_1 be respectively the n_1 measured parameters, and the r_1 parameters to be determined through χ^2 minimization. Let ξ_2 and α_2 be n_2 and r_2 additional independent parameters to be added for a second χ^2 minimization process. If the minimum χ^2 for the first step is χ_1^2 and for the second step χ^2, then the difference $\chi^2 - \chi_1^2$ is distributed as χ^2 for $n_2 - r_2$ degrees of freedom.

Proof: As usual $\chi_1^2 = \eta_1{}^\dagger P_1 \eta_1$ and $\chi^2 = \eta^\dagger P \eta$. It is convenient to increase the dimentionality of P_1 so that it operates on the full space η and to then consider the quadratic form $\eta^\dagger(P - P_1)\eta$. We extend $P_1 = (1 - g_1 G_1^{-1} g_1^\dagger)$ by adding enough zeroes to 1, g_1, and G_1^{-1} to increase the size of these matrices to dimensionality nxn, rxn, and rxr respectively where $n = n_1 + n_2$ and $r = r_1 + r_2$. For example

$$1 = \begin{pmatrix} 1 \\ (n_1 \times n_1) \end{pmatrix} \longrightarrow \left(\begin{array}{c|c} 1 & 0 \\ (n_1 \times n_1) & \\ \hline 0 & 0 \end{array}\right) \equiv P_{n1}$$

which is an nxn projection operator.

The matrix g for χ^2 is of the form

$$g = \left(\begin{array}{c|c} g_1 & 0 \\ \hline g_2 & \end{array}\right)$$

Notice that $\langle \xi_2 \rangle$ may depend on α_1 but $\langle \xi_1 \rangle$ is independent of α_2. Evidently one may write $g_1 = P_{n1} g$, $g^\dagger g_1 = g_1{}^\dagger g_1$, and $G_1^{-1} G_1 = P_{n1}$. We note that $(P - P_1)^2 = P^2 - PP_1 - P_1 P + P_1^2 = P + P_1 - PP_1 - P_1 P$. If $PP_1 + P_1 P = 2P_1$ then $(P - P_1)^2 = P - P_1$ and $P - P_1$ is a projection

operator. Actually it is sufficient to show that $PP_1 = P_1$ since then $PP_1 = P_1 = P_1^\dagger = P_1^\dagger P^\dagger = P_1 P$.

We proceed as follows:

$$PP_1 = (1 - gG^{-1}g^\dagger)(P_{n1} - g_1 G_1^{-1} g_1^\dagger)$$

$$= P_1 - gG^{-1}g^\dagger P_{n1} + gG^{-1}g^\dagger g_1 G_1^{-1} g_1^\dagger$$

$$= P_1 - gG^{-1}g^\dagger P_{n1} + gG^{-1} P_{n1} g_1^\dagger$$

$$= P_1$$

Thus $P-P_1$ is a projection operator so that $\eta^+(P-P_1)\eta$ can be represented as a sum of squares. It then follows that $\eta^+(P-P_1)\eta$ is distributed as χ^2 for some as yet undetermined number of degrees of freedom. However, $\langle \chi^2 - \chi_1^2 \rangle = \langle \chi^2 \rangle - \langle \chi_1^2 \rangle = n_1 + n_2 - (r_1 + r_2) - (n_1 - r_1)$ $= n_2 - r_2$ so $\eta^+(P-P_1)\eta$ must be distributed as χ^2 for $n_2 - r_2$ degrees of freedom.

D. Preliminary Measurements of Decay Rates

The 1968 measurement of Σ^- lifetime $\tau_- = (1.38 \pm .07) \times 10^{-10}$ sec performed by Whiteside and Gollub[21] is inconsistent with previous measurements and has been excluded from the summaries given in Tables 1 and III. In order to resolve this inconsistency we have obtained preliminary values of τ_- and τ_+ from our data. We find

$$\tau_- = (1.460 \pm .027)\times10^{-10}\text{sec} \quad \text{or} \quad \Gamma_- = (.685 \pm .013)\times10^{10}/\text{sec}$$

$$\tau_+ = (.771 \pm .014)\times10^{-10}\text{sec} \quad \text{or} \quad \Gamma_+ = (1.297 \pm .024)\times10^{10}/\text{sec}.$$

Our value of τ_- is in good agreement with that of Whiteside and Gollub and is in serious disagreement with the value used in Table I.

We have corrected our data for scanning biases and for the finite size of the bubble chamber. We have used only those events in which the momentum of the Σ is greater than 200 MeV/c and the absolute value of its dip less than 30°. We have also excluded those events having $\cos^{-1}(\hat{\Sigma} \cdot \hat{v}) > 0.9$ as measured in the Σ rest frame. The value of τ_+ was obtained using only Σ^+_+ events. In both cases the quoted uncertainty allows for a possible 1% systematic bias.

In addition to our results two preliminary measurements of τ_- were presented at the April 1969 meeting of the American Physical Society in Washington, D.C. These results are

$$\tau_- = 1.43 \times 10^{-10}\text{sec}$$ [22]

and

$$\tau_- = (1.54 \pm .06) \times 10^{-10}\text{sec}.$$ [23]

We have recalculated the results of Tables IV and V using our preliminary values of Γ_- and Γ_+. The results are given in Tables IV' and V'. The $|\Delta I| = 1/2$ triangle obtained by using our decay rates is shown in Fig. 26. Note that our values of Γ_- and Γ_+ give a better fit to the $|\Delta I| = 1/2$ rule than the values of Table I.

Table IV'. Fitted values of Σ decay amplitudes. Matrix element SP refers to the scalar-pseudoscalar interaction (21) and VA refers to the vector-axialvector interaction (22). Amplitudes A and B for the SP interaction are given in units of 10^5 $sec^{-1/2}$ and amplitudes A' and B' for the VA interaction are given in units of 10^5 GeV^{-1} $sec^{-1/2}$.

Fit	Matrix Element	$A_{11} + A_{31}/2$	$B_{11} + B_{31}/2$	A_{13}	B_{13}	A_{33}	B_{33}	Degrees of Freedom	χ^2	γ_o
7	SP	-0.899 ±0.023	29.88 ±0.37	1.984 ±0.018	-0.746 ±0.108	0	0	4	1.20	< 0
8	VA	-3.486 ±0.093	14.14 ±0.17	7.702 ±0.070	-0.352 ±0.051	0	0	4	2.59	< 0
9	SP	-0.933 ±0.037	29.57 ±0.46	2.006 ±0.027	-0.804 ±0.227	0.041 ±0.038	-0.115 ±0.352	2	0.13	< 0
10	VA	-3.713 ±0.162	13.89 ±0.23	7.852 ±0.115	-0.381 ±0.117	0.270 ±0.169	-0.062 ±0.182	2	0.13	< 0
11	SP	-0.974 ±0.048	29.15 ±0.57	2.033 ±0.033	-0.537 ±0.299	0.084 ±0.049	0.307 ±0.467	2	0.12	> 0
12	VA	-3.878 ±0.187	13.69 ±0.26	7.963 ±0.130	-0.252 ±0.137	0.445 ±0.193	0.143 ±0.214	2	0.12	> 0

Best Fitted Values of Measured Parameters for Fits 7 and 8.

Fit	α_-	α_o	α_+/α_o	Γ_-	Γ_{total}	b	Φ_-	Φ_+
7	-0.075	-0.993	-0.057	0.688×10^{10}	1.294×10^{10}	0.486	-0.69°	166.23°
8	-0.076	-0.990	-0.055	0.689×10^{10}	1.291×10^{10}	0.494	-0.69°	166.76°

Table V'. Error matrices for Σ decay amplitudes. The rows and columns are ordered as $A_{11} + A_{31}/2$, $B_{11} + B_{31}/2$, A_{13}, B_{13}, A_{33}, B_{33}.

ERROR MATRIX FOR FIT 7

.000549	.002233	-.000151	-.000015
.002233	.136699	-.001378	-.000411
-.000151	-.001378	.000323	-.000035
-.000015	-.000411	-.000035	.011730

ERROR MATRIX FOR FIT 8

.008719	.003979	-.002250	-.000022
.003979	.029675	-.002369	-.000071
-.002250	-.002369	.004862	-.000070
-.000022	-.000071	-.000070	.002572

ERROR MATRIX FOR FIT 9

.001368	.010111	-.000710	-.002246	-.001107	-.003628
.010111	.215936	-.006854	-.026446	-.010654	-.042737
-.000710	-.006854	.000712	.001673	.000762	.002773
-.002246	-.026446	.001673	.051396	.002608	.069870
-.001107	-.010654	.000762	.002608	.001468	.004161
-.003628	-.042737	.002773	.069870	.004161	.124140

Table V'. Continued.

ERROR MATRIX FOR FIT 10

.026363	.024465	-.014398	-.006806	-.022524	-.010954
.024465	.054096	-.016519	-.008930	-.025795	-.014373
-.014398	-.016519	.013273	.004893	.015502	.008009
-.006806	-.008930	.004893	.013669	.007680	.019135
-.022524	-.025795	.015502	.007680	.028468	.012258
-.010954	-.014373	.008009	.019135	.012258	.033170

ERROR MATRIX FOR FIT 11

.002277	.019964	-.001308	-.007275	-.002054	-.011638
.019964	.321968	-.013254	-.080739	-.020795	-.129148
-.001308	-.013254	.001100	.004977	.001375	.008039
-.007275	-.080739	.004977	.089223	.007853	.129846
-.002054	-.020795	.001375	.007853	.002439	.012502
-.011638	-.129148	.008039	.129846	.012502	.218195

ERROR MATRIX FOR FIT 12

.034984	.035892	-.019971	-.012683	-.031355	-.020302
.035892	.069230	-.023830	-.016656	-.037382	-.026662
-.019971	-.023830	.016814	.008693	.021109	.014054
-.012683	-.016656	.008693	.018781	.013716	.027239
-.031355	-.037382	.021109	.013716	.037359	.021847
-.020302	-.026662	.014054	.027239	.021847	.045909

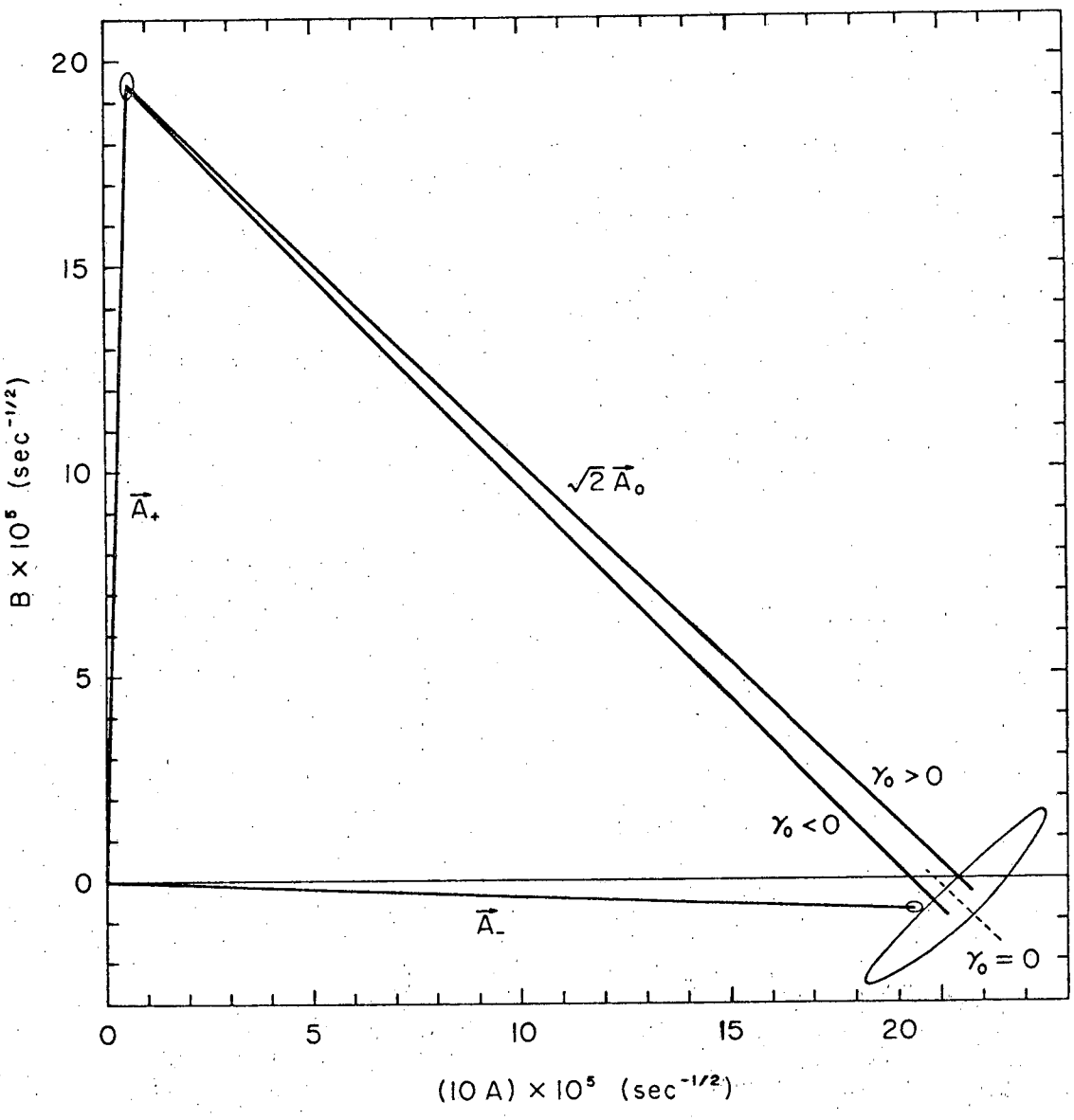

XBL 697-865

Fig. 26. The $\Delta I = 1/2$ triangle obtained by using the new decay rates.

REFERENCES

1. M. Gell-Mann and A. Pais, The Proceedings of the 1954 Glasgow Conference on Nuclear and Meson Physics (Pergamon Press, London and New York, 1955), p. 342.

2. H. Sugawara, Phys. Rev. Letters 15, 870, 997 (1965); M. Suzuki, Phys. Rev. Letters 15, 986 (1965).

3. Particle Data Group, Rev. Mod. Phys. 41, 109 (1969). See, however, Appendix D.

4. M. B. Watson, M. Ferro-Luzzi, and R. D. Tripp, Phys. Rev. 131, 2248 (1963).

5. N. Horwitz, J. J. Murray, R. R. Ross, and R. D. Tripp, Lawrence Radiation Laboratory Report UCRL-8269.

6. M. Ross and G. Shaw, Ann. Phys. (N.Y.) 13, 147 (1961).

7. J. K. Kim, Phys. Rev. Letters 19, 1074 (1967).

8. F. T. Solmitz, A. D. Johnson, and T. B. Day, Alvarez Group Programming Note P-117 (Lawrence Radiation Laboratory, October 1965) (Unpublished).

9. O. I. Dahl, T. B. Day, F. T. Solmitz and N. L. Gould, Alvarez Group Programming Note P-126 (Lawrence Radiation Laboratory, July 1968) (Unpublished).

10. Private communication. However the values used by us are very similar to those determined by the analysis of M. H. MacGregor, R. A. Arndt, and R. M. Wright, "Determination of the Nucleon-Nucleon Scattering Matrix X. (p,p) and (n,p) Analysis from 1-450 MeV," (to be published in Phys. Rev.).

11. V. Bargmann, L. Michel, and V. L. Telegdi, Phys. Rev. Letters 2, 435 (1959).

12. For example violation of unitarity at high energies. For more details see S. Gasiorowicz, Elementary Particle Physics (John Wiley & Sons, Inc., New York, 1966), PART IV.

13. E. Merzbacher, Quantum Mechanics (John Wiley & Sons, Inc., New York, 1961), Chap. 22.

14. J. D. Bjorken and S. D. Drell, Relativistic Quantum Mechanics (McGraw-Hill Book Company, New York and San Francisco, 1964).

15. J. P. Berge, Proceedings of the XIIIth International Conference on High Energy Physics (University of California Press, Berkeley and Los Angeles, 1967), p. 46.

16. C. Jarlskog, Nucl. Phys. B3, 365 (1967).

17. We use the compilation of J. M. McKinley, Rev. Mod. Phys. 35, 788 (1963), with some cognizance of the higher energy analysis of P. Bareyre, C. Brickman, A. V. Stirling, and G. Villet, Phys. Letters 18, 342 (1965), to estimate the following phase shifts:

$\delta_1 = +9$ deg, $\delta_3 = -12$ deg, $\delta_{11} = 0$ deg, and $\delta_{31} = -3$ deg. Each phase shift has an uncertainty of about 1.5 deg. The $|\Delta I| = 1/2$ analysis described here is quite insensitive to these small phase shifts.

18. M. Bazin, H. Blumenfeld, U. Nauenberg, L. Seidlitz, R. J. Plano, S. Marateck, and P. Schmidt, Phys. Rev. 140, B1358 (1965). See, however, R. D. Young, M. Sugawara, and T. Sakuma, Phys. Rev. 145, 1181 (1966).

19. W. E. Humphrey, B. J. Cottrell, Alvarez Group Programming Note P-6 (Lawrence Radiation Laboratory, March 1966) (Unpublished).

20. F. T. Solmitz, Ann. Rev. Nucl. Sci., 14, 375 (1964).

21. H. Whiteside and J. Gollub, Nuovo Cimento 54A, 537 (1968).

22. H. Taft, Bull. Am. Phys. Soc. 14, 484 (1969).

23. R. A. Burnstein, H. A. Rubin, and E. L. Erickson, Bull. Am. Phys. Soc. 14, 500 (1969).

TECHNICAL INFORMATION DIVISION
LAWRENCE RADIATION LABORATORY
UNIVERSITY OF CALIFORNIA
BERKELEY, CALIFORNIA 94720